IEEE Access
Multidisciplinary | Rapid Review | Open Access Journal

Received 20 June 2024, accepted 19 July 2024, date of publication 29 July 2024, date of current version 27 August 2024.

Digital Object Identifier 10.1109/ACCESS.2024.3435528

RESEARCH ARTICLE

Leaf-Shaped Antennas for Sub-6 GHz 5G Applications

TAPAN NAHAR[1], SANYOG RAWAT[2], PARUL PATHAK[3], PRAMOD KUMAR[4], (Senior Member, IEEE), AND JAUME ANGUERA[5]

[1]Department of Information and Communication Technology, Marwadi University, Rajkot 360003, India
[2]Department of Electronics and Communication Engineering, Central University of Rajasthan, Ajmer 305817, India
[3]Department of Electronics and Communication Engineering, JECRC University, Jaipur 303905, India
[4]Department of Electronics and Communication Engineering, Manipal Institute of Technology, Manipal Academy of Higher Education, Manipal 576104, India
[5]Electronics and Communications Department, Universitat Ramon Llull, 08022 Barcelona, Spain

Corresponding authors: Pramod Kumar (p.kumar@manipal.edu) and Sanyog Rawat (sanyog.rawat@curaj.ac.in)

This work was supported by the Manipal Academy of Higher Education, Manipal, India.

ABSTRACT The research community has been more interested in nature-inspired antenna solutions in recent years. Well-known organizations all around the world have set up labs to investigate the structures, operations, and traits of creatures that exist. One valuable method is investigating geometrical depictions of biological shapes, including fractal shapes and polarized geometry. This paper focuses on the design of a leaf-shaped antenna, its 4 × 1 corporate-fed array, spatial diversity Multiple Input Multiple Output (MIMO) antenna, and pattern diversity MIMO antenna, which operate in the sub-6 GHz range and specifically cover the 5G bands: N77 (3.3–4.2 GHz), N78 (3.3–3.8 GHz), and N79 (4.7 GHz) (4.4–5 GHz). The radiating element of the array is modeled like a natural plant leaf, and a defective ground plane is used to reduce size and increase bandwidth. To obtain dual band characteristics and circular polarization, a diagonal slot in the parasitic metallic elliptical disc in the ground plane is used. A corporate feed network is used in a 4 × 1 array for excitation to radiating elements and to generate high gain performance by ensuring little reflection loss and good impedance matching. An electromagnetically coupled hexagonal array is used in a T shape between the inter-elements to reduce mutual coupling and increase the gain of the 4 × 1 array. The proposed multiband antenna array reflects less than 10% of the power between 3.4–4 GHz and 4.51–5.2 GHz and achieves a maximum gain of 6.55 dB with variations of less than 3 dB across the full operating band. MIMO configurations are required to increase the network capacity. Spatial diversity and pattern diversity MIMO antennas are designed to provide good diversity performance and sufficient isolation bandwidth. All the proposed antennas are fabricated on a commercially available FR4 substrate with a dielectric constant of 4.3 and a height of 1.6 mm, making them inexpensive for mass production. The performance of fabricated antennas is compared with that of simulated antennas. Compact size, planar design, broad bandwidth, and stable gain make the proposed antennas suitable for sub-6 GHz 5G applications.

INDEX TERMS Sub 6 GHz antenna, 5G (fifth generation), nature inspired antenna, MIMO, corporate fed antenna array.

I. INTRODUCTION

The compact multiband planar antenna design for sub-6 GHz 5G communication is a crucial problem for antenna designers since keeping other characteristics like moderate gain and broad bandwidth while remaining compact is difficult. As small wireless devices are in high demand, compact antenna design is essential [1]. Due to the obvious long working wavelength (λ), the size of the antenna in the sub-6 GHz band is increasing. As size reduction techniques are applied, antenna gain and efficiency are lowered owing to reduced effective aperture area, making achieving the required radiation performance difficult [2], [3]. As the number of mobile phone operators grows exponentially,

The associate editor coordinating the review of this manuscript and approving it for publication was Qi Luo.

internet connection speed and mobile data requirements become a significant problem for today's wireless systems [4]. Fifth-generation technology is distinguished by its ability to accommodate a large number of concurrent users, increase network capacity, improve data rates in Gbps, reduce transmission latency in milliseconds, and reduce costs [5]. For 5G communication, the ITU (International Telecommunication Union) has allocated microwave bands (3.4-3.6 GHz and 5-6 GHz) and mm-wave bands (24.25-27.5 GHz, 37-40.5 GHz, and 66-76 GHz), while the FCC (Federal Communications Commission) has specified a spectrum option of 27.5-28.35 GHz [6], [7]. Communication in mm-wave bands has various challenges, including fading, environmental absorptions and attenuations, and a low signal-to-noise ratio. As implementing mm-wave communication devices in existing base stations is highly expensive, most telecom operators are updating existing sub-6 GHz base stations and attempting to improve service quality. The basic option of bands in sub-6GHz 5G connectivity is N77 3.7 GHz (3.3–4.2 GHz), N78 3.5 GHz (3.3–3.8 GHz), and N79 4.7 GHz (4.4–5 GHz) [7], [8]. Many nations, including South Korea, the European Union, the United States, China, and Japan, are using or proposing to employ LTE (Long Term Evolution) bands 42 (3.4–3.6 GHz) and 43 (3.6–3.8 GHz) as pioneer 5G bands [7], [8], [9].

In the literature, many compact multiband microwave antennas have been reported. [10] shows a sub-6 GHz antenna with two parallel printed dipoles. To increase impedance matching, an H-shaped groove is cut into the ground. For frequency reconfigurable properties, P-I-N diodes are utilized between the feeding structure and the dipoles. The proposed antenna has a decent bandwidth and modest gain, but its large size is a major disadvantage. [11] describes a folded slotted resonant cavity-based antenna. The proposed antenna has a modest size of $0.24\lambda \times 0.24\lambda \times 0.07\lambda$ and a constant gain, but its main disadvantages are its short bandwidth and non-planar shape. [7] shows a circular patch antenna with a defective ground construction. To get the requisite operating band, a rectangular slit is constructed in partial ground. The proposed antenna has a good bandwidth, a compact size, and a planar shape; however, the gain fluctuation is more than 3 dB. [12] presents a step impedance resonator-based antenna for multiband 2.4 GHz/5.8 GHz applications. The proposed antenna has a limited bandwidth, a low gain, and a huge size, but the stepped impedance-based filtering structure is new. [13] shows an optically transparent dual-band antenna. The proposed antenna has dual-band operation and excellent bandwidth, although the gain in one band is minimal. The antenna is likewise rather large. [14] proposes a slotted printed dipole antenna for multiband operation. It is fed by a coplanar waveguide. To minimize the size, two symmetrically folded slots are employed. A rectangular feed line with a step form and a rectangular ground plane are employed. The proposed antenna functions in the multiband frequencies of 1.9–2.17 GHz, 3.4–3.6 GHz, and 5.15–5.35 GHz and has a modest size of $0.19\lambda \times 0.21\ \lambda \times 0.005\lambda$. Gain varies widely, and at some points in the working band, gain is negative. [1] proposes a slotted patch and two inverted F-shaped defective ground structure-based antennas for multiband applications at 2.51 GHz, 5.26 GHz, and 8.18 GHz. The proposed antenna is small and multiband, although its gain varies greatly. It is difficult to achieve small dimensions, wide bandwidth, steady gain, planar shape, and modest gain for a sub-6 GHz antenna at the same time.

Nature-inspired design was chosen to meet the aforesaid research gap. The incorporation of nature-inspired architecture into technological and scientific issues is a hot topic among researchers worldwide. Leading educational establishments like the Massachusetts Institute of Technology and Harward University have begun setting up research labs to study how engineering behavior and architecture are influenced by nature and produce extraordinary results [15]. The inner structures and outside. anatomy of animals serve as a major source of inspiration for antenna design, as these elements function similarly to the antennas found in systems for communicating. For a variety of bands and technological advances, scientists are experimenting with antennas with bio-inspired plant geometries that incorporate plant elements, including branches, leaves, and petals. Because of their potential outcomes, leaf-shaped antennas—which are designed like leaves—have drawn attention. Identical to dish antennas, leaves possess a light-gathering center that exhibits intricate and fractal-like features [15], [16]. These kinds of antennas are a viable option for small, barely noticeable antennas since they are designed to collect solar energy for photosynthetic purposes. In contrast to classical shapes, the nature-inspired antenna exhibits a larger density of surface current in a narrower region. Several articles published demonstrate these antennas' potential. In comparison to the circular design, the leaf-shaped design exhibits a decrease in overall length of 33.61% and breadth of 52.01% [16]. Featuring a highest gain of 18.66 dBi, the hyperbolic partial sinusoidal curved leaf antenna delivers a broad bandwidth of 8.92 THz [17].

The patch's shape is inspired by the shape of a leaf. Naturally occurring plants have strong radiation-collecting capacity or good EM (electromagnetic) wave-receiving ability. Due to their structure [16], [18], [19], [20]. To minimize size while increasing bandwidth, a partial ground plane is employed. A diagonally slotted parasitic disc is employed below the patch in the ground plane to achieve dual band operation, gain stability, and circular polarization.

Aside from 5G mobile communication, the proposed antenna supports a wide range of biomedical applications, including medical monitoring applications, patient motion tracking, wireless vital sign monitoring, pharmaceutical storage monitoring, cancer detection, cardiology imaging, pneumology imaging, obstetrics imaging, ear-nose-throat imaging, measurements in underwater medicine, space

medicine, sport medicine, military medicine, emergency medicine, rubble rescue radar, biofeedback-based rehabilitation procedures such as respiratory rehab, cardiovascular rehab, and occupational therapy, the control of artificial prostheses and the actuation of wheelchair driving systems, smart-home systems and many more. The proposed antenna can potentially be employed as a medical implant therapy device. The antenna can be utilized as therapy and communication equipment. The applicability of the suggested antenna for early breast cancer detection is thoroughly examined in this research. Researchers face significant challenges in developing small antennas with excellent gain and wide bandwidth at μ-Wave spectrum. The sub-6 GHz bands' half wavelengths extend from 30 mm (5 GHz) to 52 mm (3 GHz). When the antenna dimension is less than 52 $\times$ 52 square mm, the antenna gain is lowered at lower frequencies. Dimension reduction approaches must be used while maintaining other factors like as gain and efficiency [21].

Initially, a dual-band leaf-shaped nature-inspired antenna of 25$\times$20 $\times$ 1.6 (0.24$\lambda\times$0.20 $\lambda\times$0.015 λ) mm3 is proposed in this paper, which works from 2.95-3.8 GHz and 4.25-4.95 GHz with a gain of 1.57-1.68 dBi. A four-element corporate fed array is presented, which increases gain by about four times. MIMO configurations are necessary in 5G communication to enhance network capacity, service quality, and mitigate the impacts of multipath propagation. Pattern diversity and spatial diversity-MIMO configurations of the leaf-shaped antenna are illustrated.

This paper is divided into six sections. Section I covers a literature survey and research gaps related to sub-6 GHz antennas. The design and performance of a single antenna are presented in Section II. Section III presents a 4 $\times$ 1 corporate-fed array of leaf-shaped antennas and its results. Spatial diversity and pattern diversity of MIMO antennas are discussed in Section IV. The paper concludes in Section V.

II. EVOLUTION OF SINGLE ANTENNA ELEMENT

A. ANTENNA DESIGN

On the CST (Computer Simulation Technology) microwave studio, a leaf-shaped patch was simulated for the 5G sub-6 GHz spectrum. Because of its ease of availability and inexpensive cost, a FR4 substrate with a dielectric constant of 4.3, a loss tangent of 0.025, and a thickness of 1.6 mm was chosen. FR4 stands for flame retardant 4, which is a glass-reinforced epoxy resin laminate. FR4 is good option for the low frequencies. It's losses increase with increasing frequencies. It is suitable for general use but not ideal for high-frequency or high-temperature environments. It is easy to fabricate but not eco-friendly. Due to its modest size, the suggested antenna, FR4, is made for simple installation without the need for pricey flexible substrates. The copper layer thickness is 0.035 mm for the patch as well as the ground. The patch is energized using microstrip line feeding. To achieve dual-band operation, a partial ground plane is employed on the reverse side of the substrate, and a diagonally slotted elliptical metallic layer is introduced. Initially, a patch in the shape of a leaf is created using (1) [22].

$$r = 2a(1 + \cos(\theta)) \tag{1}$$

(1) is written in polar form. Cartesian coordinates may be computed using following (2) and (3) [22].

$$x = r\cos(\theta) \tag{2}$$

$$y = r\sin(\theta) \tag{3}$$

Using these equations, a cardioid form is produced by entering different values of θ from 0 to 360 degrees and r of 10 mm, whose top point is changed or displaced to 14.04 mm to obtain the geometry in the form of a leaf. One may achieve clearer geometry as the number of points increases. When utilizing a partial ground plane, the feed line's length is shortened from the initial choice of half wavelength. Here are the optimized dimensions presented in Fig. 1 (a).

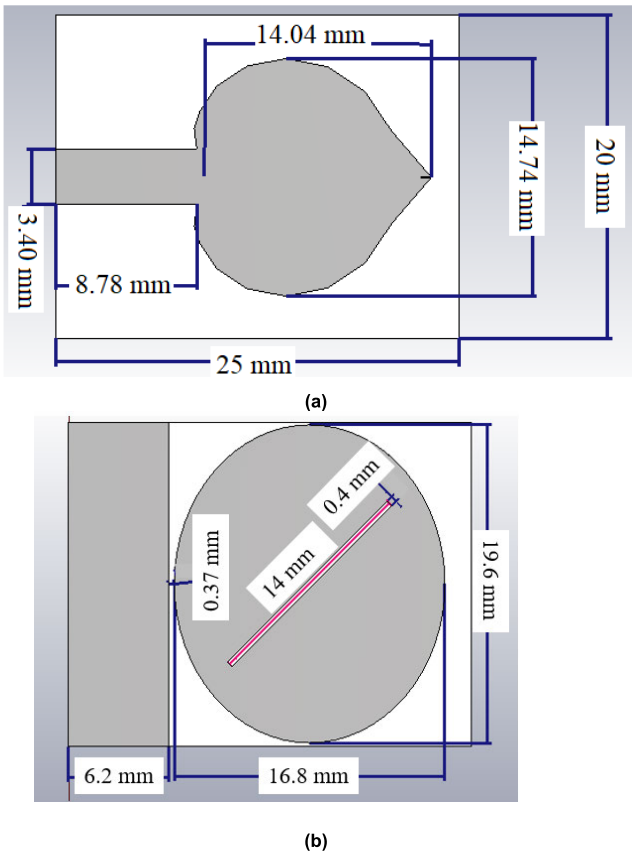

FIGURE 1. Geometry of leaf shaped Sub-6 GHz antenna (a) Front view (b) Back view.

To achieve a compact size and the necessary band of operation, the dimension of the leaf-shaped patch is lowered by changing the partial ground plane length. In order to accomplish dual band functioning and circular polarization,

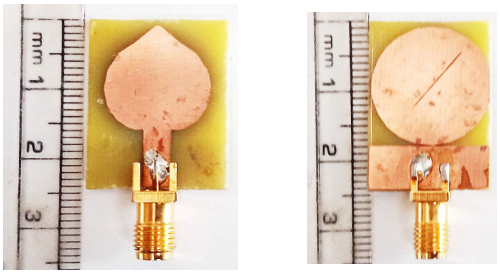

(a) (b)

FIGURE 2. Fabricated prototype of leaf shaped antenna (a) Front view (b) Back view.

a diagonally slotted elliptical metallic layer is applied to the ground plane. Fig. 1 depicts the optimized design parameters and antenna shape. Fig. 2 (a) and (b) show the front and rear views of the fabricated prototype antenna.

B. PERFORMANCE AND DISCUSSION

Fig. 3 depicts the simulated and measured reflection coefficient (S11) of the proposed leaf-shaped antenna. It may be observed that the simulated leaf-shaped antenna resonates at dual frequencies of 2.94–3.81 GHz and 4.24–4.95 GHz, with impedance bandwidths of 24.16% and 15.10% at 3.6 GHz and 4.7 GHz, respectively. From 3 GHz to 3.9 GHz and 4.3 GHz to 5 GHz, the measured reflection coefficient (S11) is less than -10 dB. At 3.6 GHz and 4.77 GHz, the minimum measured reflection coefficient (S11) is −16 dB and −22 dB, respectively. It is possible to see that the manufactured antenna covers all of the necessary bands while providing some lower impedance matching and return loss performance. It might be due to certain irregularities in the manufacturing around the edges.

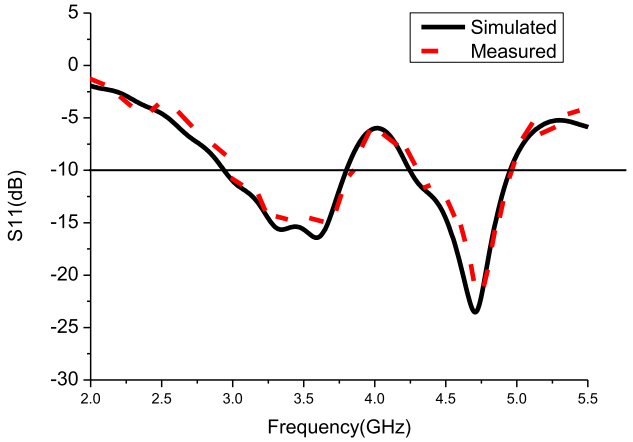

FIGURE 3. Reflection coefficient (S11) variations with frequency of Leaf shaped antenna.

The fabricated antenna's radiation pattern has been measured in an anechoic chamber, as shown in Fig. 4. Fig. 5(a) depicts a consolidated radiation pattern of simulated and measured E and H fields at 3.6 GHz.

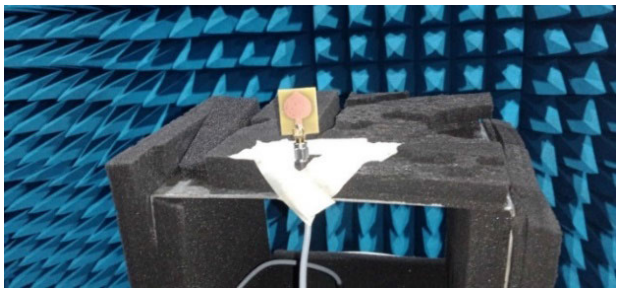

FIGURE 4. Fabricated prototype in an anechoic chamber for radiation pattern measurement.

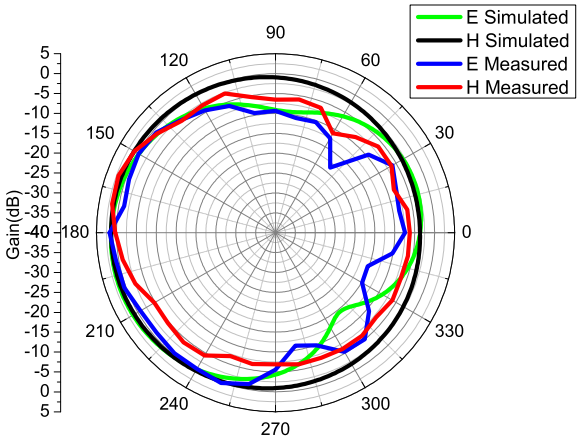

(a)

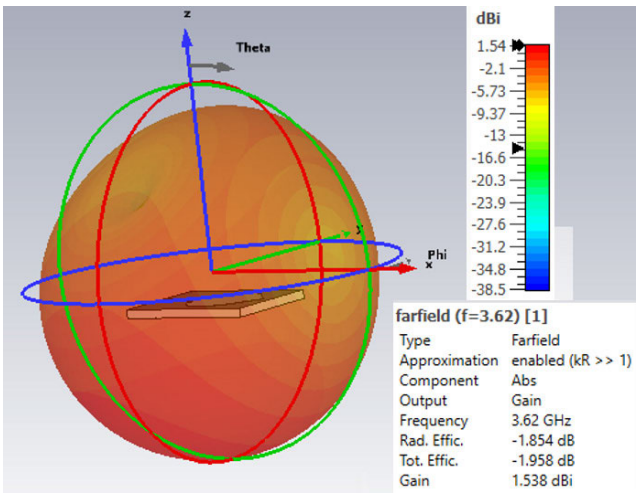

(b)

FIGURE 5. (a) Consolidated simulated and measured E field and H field radiation pattern at 3.6 GHz (b) Three dimensional simulated radiation pattern at 3.6 GHz.

At phi = 0, the proposed antenna has maximum radiation on the ground plane side and a relatively tiny minor lobe. At phi = 90 degrees, there is good coverage. It can be seen that the shapes of the simulated and measured patterns are

similar to some extent. It is possible to see that the measured radiation pattern has lower side lobe values.

The maximum simulated and measured gains of the proposed antenna are 1.5 dB and 1.7 dB, respectively, at phi = 0 deg. and 1.3 dB and 1.9 dB at phi = 90 deg. It can be seen from Fig. 5 (b) that the three-dimensional radiation pattern has a maximum gain of 1.5 dBi at 3.6 GHz.

Fig. 6(a) depicts the simulated and measured radiation patterns at 4.7 GHz. It can be seen that simulated patterns and measured patterns are extremely closely related. The principal lobes are almost matched, but the measured antenna's rear lobe is smaller than the simulated one. The maximum simulated and measured gain is 1.79 dB and 1,98 dB at 4.7 GHz, respectively. It can be seen from Fig. 6(b) that a three-dimensional radiation pattern has a maximum gain of 1.79 dBi at 4.7 GHz.

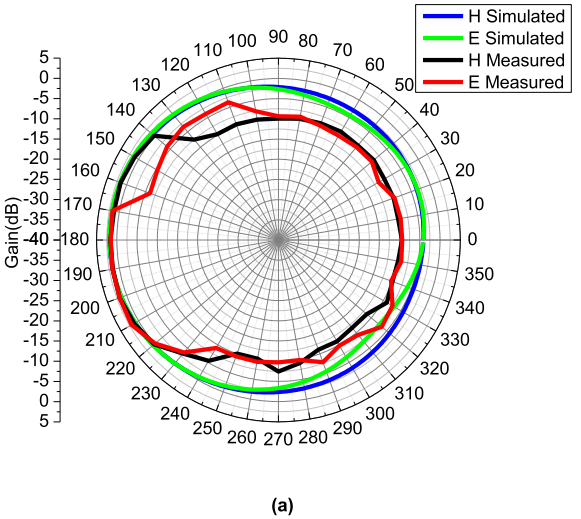

(a)

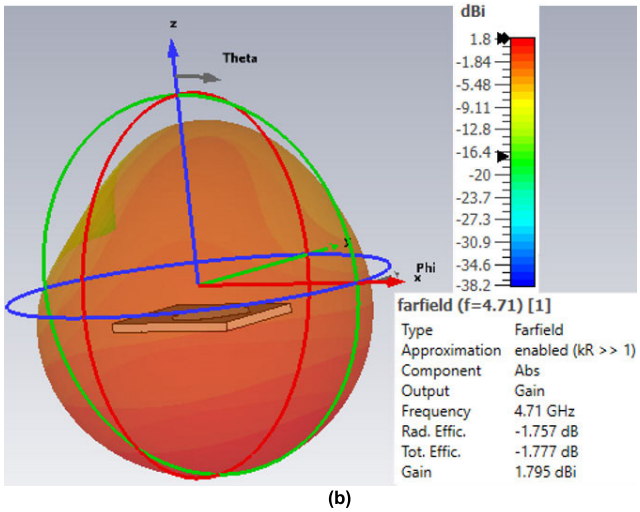

(b)

FIGURE 6. (a) Consolidated simulated and measured E field and H Field radiation pattern at 4.7 GHz (b) Three dimensional radiation pattern at 4.7 GHz.

Fig. 7 (a) and (b) show variations in gain in the first operating band and the second operating band, respectively. At 3.6 GHz and 4.7 GHz, the gain of the leaf-shaped antenna

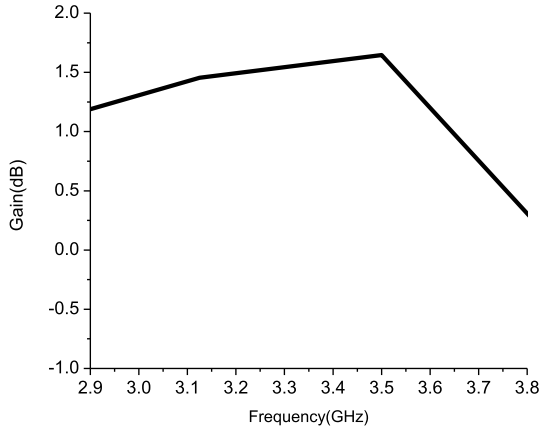

(a)

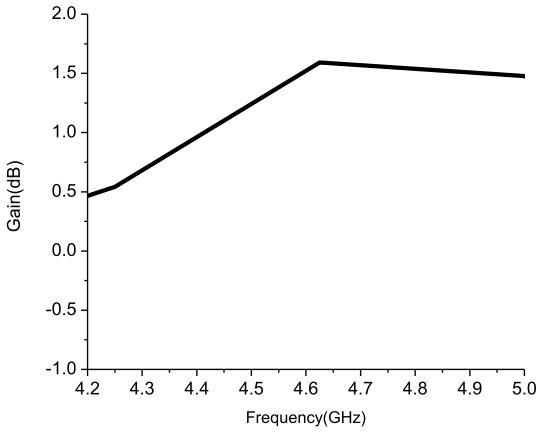

(b)

FIGURE 7. Gain of leaf shaped antenna (a) for first operating band (b) for second operating band.

is 1.64 dB and 1.54 dB, respectively. Gain varies by less than 3 dB throughout working bands. Since the antenna's gain is lowered in the non-operating band, this suggests its out-of-band rejection capability. Fig. 8(a) and (b) depict the total efficiency and radiation efficiency variations with respect to frequency of the proposed leaf-shaped antenna in the first operating band and second operating band, respectively. Total efficiency and radiation efficiency are both between 65 and 70 percent in the first band and 60 to 70 percent in the second band. Since the antenna's efficiency is lowered in the non-operating band, this shows its out-of-band rejection capability. Fig. 9 shows the axial ratio versus frequency of a leaf-shaped antenna, respectively. Because the axial ratio is less than 3 dB between 4.16 and 4.62 GHz, the antenna produces circular polarization in this band. The antenna delivers linear polarization in the first band.

C. PERFORMANCE ANALYSIS OF LEAF SHAPED ANTENNA

A leaf-shaped antenna's functionality is assessed by comparing its performance at each stage after each change. All antenna iterations have the same top shape. The bottom

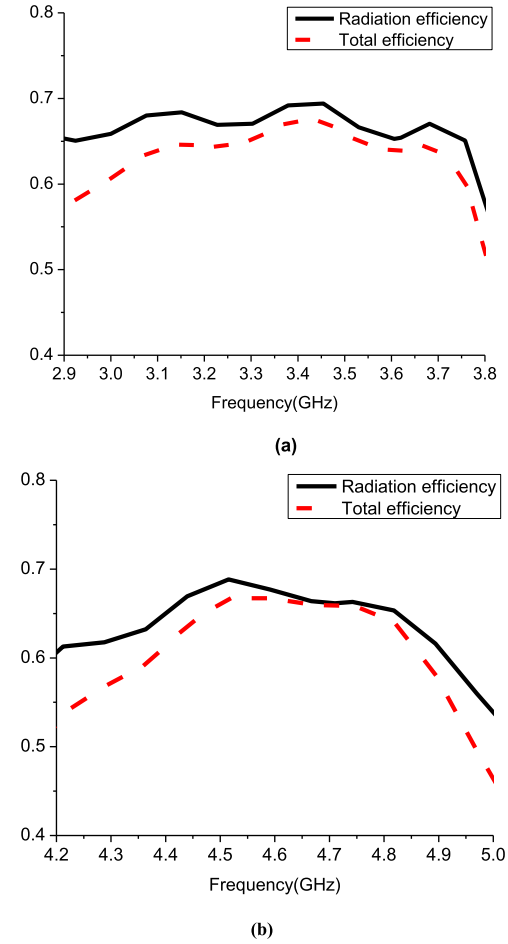

FIGURE 8. Total efficiency and radiation efficiency variations (a) in first operating band (b) in second operating band.

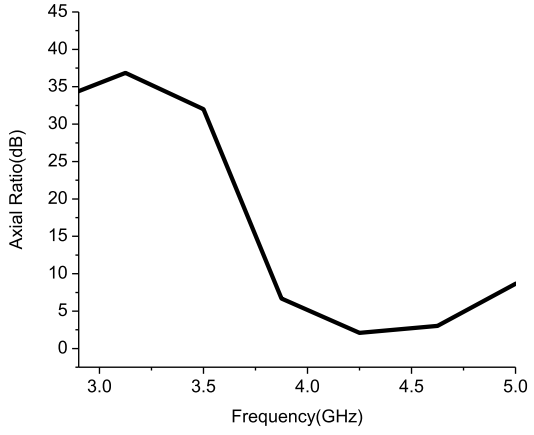

FIGURE 9. Axial Ratio variations of leaf shaped antenna.

geometry has been adjusted and is seen in Fig. 11. The suggested antenna's default ground structure is shown in Fig. 11(a). The rear side of Fig. 11 (b) is identical except for the diagonal slot. There is no slotted elliptical disc in the ground in Fig. 11 (c). Fig. 11 (d) depicts a whole ground plane on the reverse side.

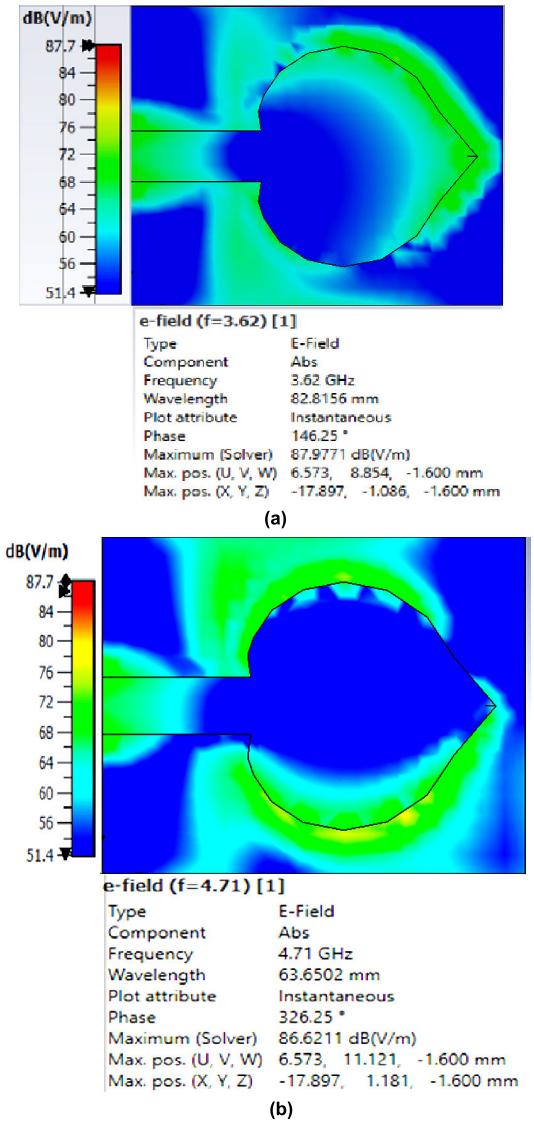

FIGURE 10. Electric field distribution of leaf shaped antenna (a) at 3.6 GHz (b) at 4.7 GHz.

Fig. 12 depicts the effect of different adjustments on the reflection coefficient (S11). When complete ground is applied, the working frequencies are not between 2 and 5 GHz. At frequencies below 6 GHz, a small antenna design is one of the objectives. Partial ground is employed, as indicated in Fig. 11(c), without a disc.

It should be noted that while employing partial ground, operational frequencies are obtained between 2.75 and 5 GHz. Notably, broad-band performance is attained. A dual-band antenna with high gain that operates at both 3.60 GHz and 4.80 GHz is needed. A metallic disc is inserted into the ground by removing a slit, as shown in Fig. 11 (a). It should be mentioned that the suggested antenna without a slot functions in a single band with a bandwidth ranging from 3 GHz to about 4.5 GHz. On the ground side of the metallic disc, a rectangular slit is created

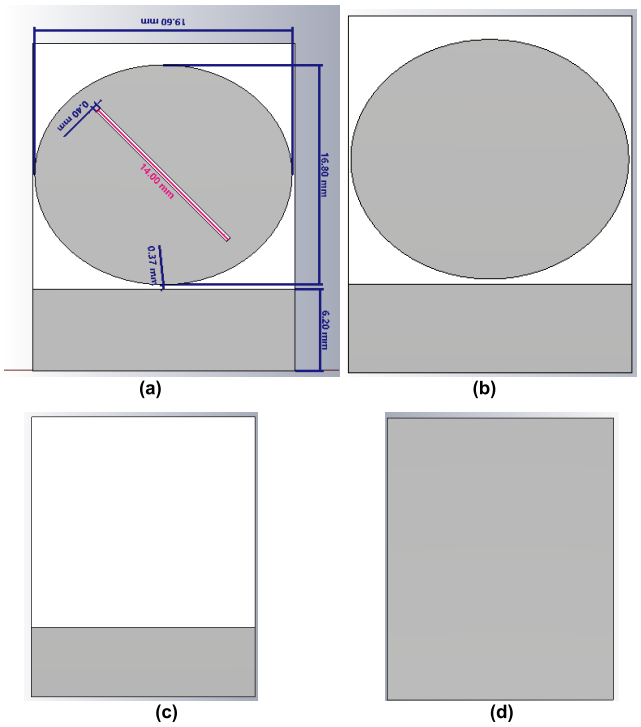

FIGURE 11. (a) Bottom view of leaf shaped antenna (b) Bottom view of proposed antenna without slot in disc (c) Partial ground and no metallic disc at back side (d) Full ground plane at back side.

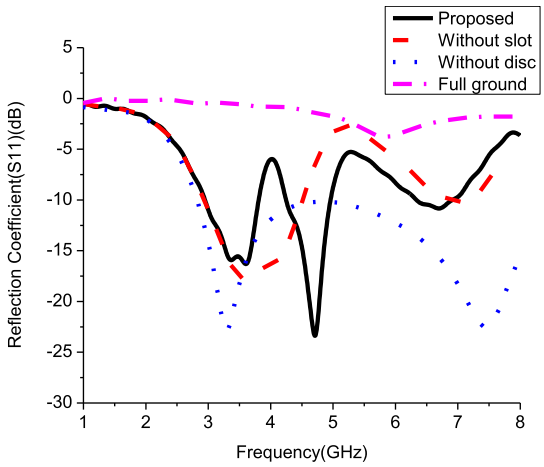

FIGURE 12. Comparisons of reflection coefficient (S11) variations with frequency for various iterations.

diagonally, resulting in a dual-band antenna that operates in two sub-6 GHz bands: 2.94–3.81 GHz and 4.24–4.95 GHz.

Fig. 13(a) and (b) depict comparisons of gain variations for the suggested leaf-shaped antenna in the first and second bands. When using the entire ground, the antenna is not operating between 3 and 5 GHz, so the gain is negative in both bands. Gain is enhanced at lower frequencies when partial ground is utilized, although bandwidth is relatively high. The gain is lowered after 3.5 GHz when a disc is introduced into the ground. When a slotted metallic disc is used, the gain is lowered but remains steady in the operating

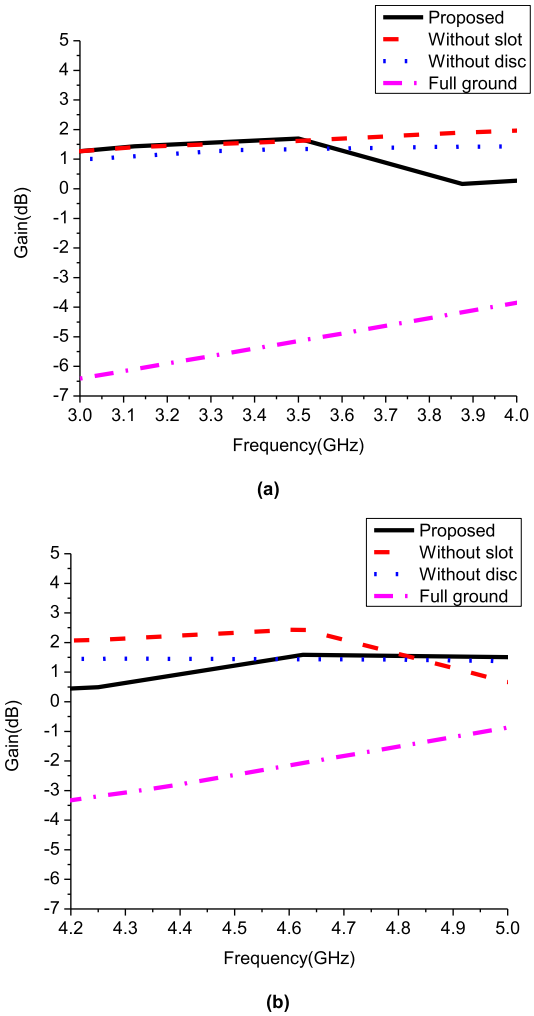

FIGURE 13. Comparisons of gain for various iterations.

band. In the second band, maximum gain is achieved when a disc without a diagonal slit is used in the ground plane. Without a disc in the ground plane, antenna gain is stable in the second band. The proposed antenna with a slotted disc has some less gain but less than 3 dB variations in the second band.

Fig. 14 illustrates axial ratio (AR) variations with frequency for all iterations of the proposed antenna. It should be noticed that the AR is more than 3 dB at all frequencies for all antenna geometries except the suggested antenna. To achieve circular polarization, a diagonallyd be noticed that the AR is more than 3 dB at all frequencies for allthe ground. geometrietoxcept the suggested antenna. placed slit is inserted in the elliptically formed metallic disc in ground. From 4.16 and 4.62 GHz, the AR becomes smaller than 3 dB, suggesting that the antenna delivers circular polarization in this band. The radiation characteristics of all iterations at 3.6 GHz for Phi = 0 and Phi = 90 degrees are compared in Fig. 15 (a) and (b).

It is to be observed that a unidirectional radiation characteristics exists above the top layer of the antenna when

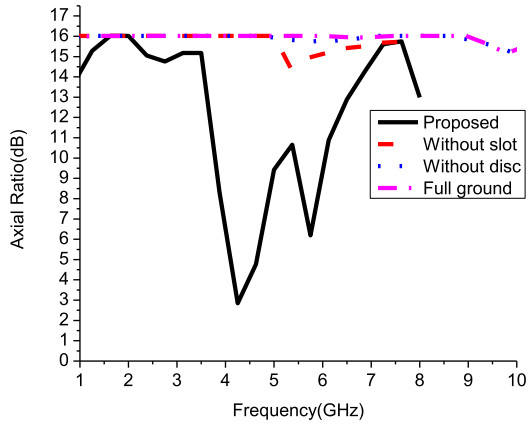

FIGURE 14. Comparisons of AR variations with frequency of various iterations of leaf shaped antenna.

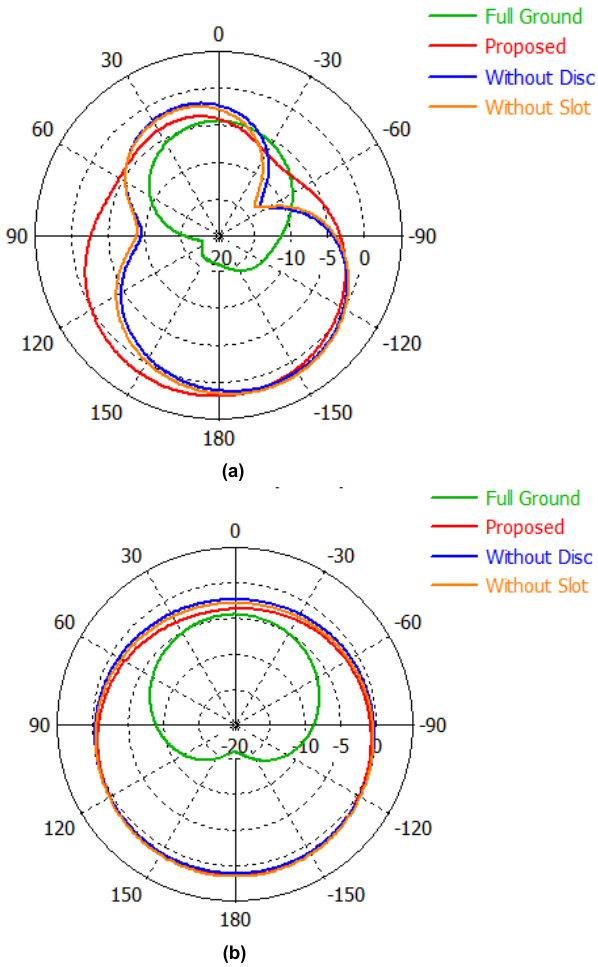

FIGURE 15. Comparisons of radiation characteristics of various iterations at 3.6 GHz (a) at Phi = 0 (b) at Phi = 90.

the full ground is used. When employing a partial ground, the radiation characteristics is altered into a semi-bidirectional pattern for Phi = 0 and Phi = 90 degree due to the absence of a ground reflecting layer. When an elliptical-shaped metallic disc is inserted into the ground plane, maximum radiation is moved back with an increase in gain. The suggested antenna provides wide coverage and gain increase in the direction of the primary lobe when a slot is carved from a metallic disc.

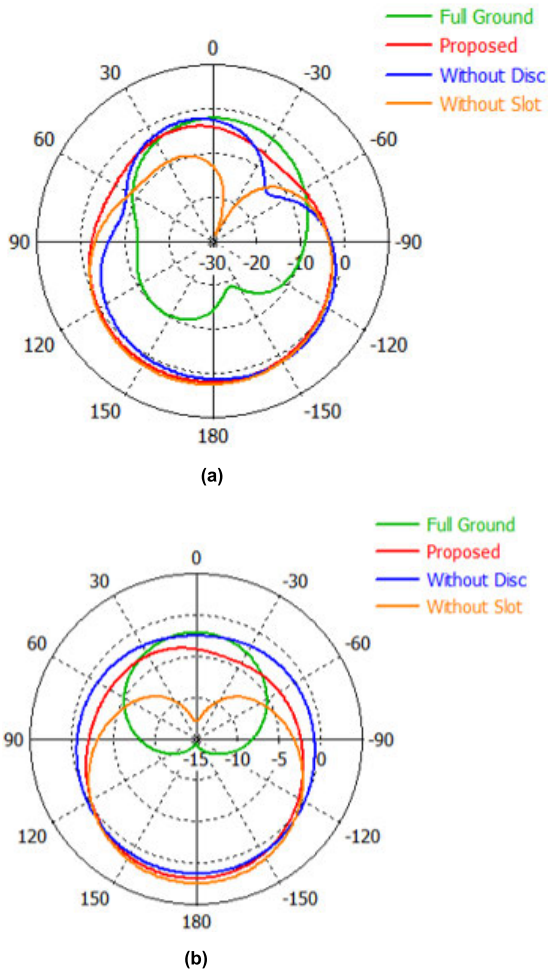

FIGURE 16. Comparisons of radiation characteristics of various iterations at 4.7 GHz (a) at Phi = 0 (b) at Phi = 90.

Fig. 16 (a) and (b) exhibit comparisons of radiation characteristics at 4.7 GHz for all iterations for Phi = 0 and 90 degree. In compared to all other geometries, the proposed antenna has the smallest minor lobe magnitude, the largest major lobe magnitude, and the widest HPBW.

D. PERFORMANCE COMPARISION WITH REPORTED ANTENNAS

Table 1 compares the proposed leaf-shaped antenna's performance to that of reported sub-6 GHz 5G antennas. The recommended antenna is tiny in comparison to maximum working wavelength and published antennas [1], [7], [10], [11], [12], [13], [14], [23], [24], [25]. The proposed antenna has a greater bandwidth than existing antennas [1], [10], [11], [12], [13], [14], [23], [24], [25], [26]. Some of the reported antenna's bandwidth is bigger than that of the planned antenna, but its gain is less. Despite its small size

TABLE 1. Performance comparison of the proposed leaf-shaped antenna with reported sub-6 GHz 5G antennas.

Work	Size	Frequency range	Impedance Bandwidth (S11<10)	Max. gain (dB)	Polarization
Proposed leaf shaped antenna (Simulated)	25*20*1.6 (0.24λ×0.20 λ×0.015 λ)	2.95-3.8 4.25-4.95	23.67%(3.6 GHz) 14.89%(4.7 GHz)	1.68(3.6) 1.57(4.7)	2.98-3.8 (linear) 4.25-4.62 GHz circular
Proposed leaf shaped antenna (Measured)	25*20*1.6 (0.24λ×0.20 λ×0.015 λ)	3-3.9 4.3-5	25.35%(3.6 GHz) 14.67%(4.77 GHz)	1.98(3.6) 1.98(4.7)	-
[10]	50*50 (0.51λ×0.51 λ)	2.89-4.07 5.1-6.19	33.7%(3.5 GHz)	2.5	linear
[11]	30*29*9 (0.238λ×0.23 λ×0.07 λ)	2.38-2.77	16.25(2.4 GHz)	1.42	dual
[7]	20*28*1.6 (0.2λ×0.28 λ×0.016 λ)	3.05-5.82	79.14(3.5 GHz)	0.34	linear
[12]	45*64 (0.36λ×0.52 λ)	2.45 5.8	4.5 3.8	-1.8 1.1	Linear
[13]	40*40*1.124 (0.33λ×0.33 λ×0.009 λ)	2.36-2.74 5.14-6.18	15.57(2.4 GHz) 18.90(5.5 GHz)	0.74 2.3	Linear
[14]	30*34*0.8 (0.19λ×0.21 λ×0.005λ)	1.9-2.17 3.4-3.6 5.15-5.35	13.5(2 GHz) 5.71(3.5 GHz) 4(5 GHz)	-1 1 3.5	linear
[1]	24*20 (0.19λ×0.156 λ)	2.35-2.47 5.08-5.36 8.01-8.31	5(2.4) 5.3(5.26) 3.66(8.18)	1.2 to 3.18	Linear
[23]	20*30*0.2 (0.22 λ×0.33 λ×0.002 λ)	3.05-3.74	20.90(3.3)	2.2	Linear
[25]	0.69 λ × 0.34 λ × 0.009 λ	3.36-3.6	6.85(3.5)	2.13-4.93	Linear
[26]	150*75*6	3.4-3.6	5.71(3.5)	5.7	Linear
[24]	136*68*1	3.4-3.8	11.11(3.6)	-	-

and large bandwidth, the suggested antenna has a higher gain than [7], [11], [12] but a lower gain than [10], [23], [24], [25], [26]. The proposed antenna features a single layer, planar design, and circular polarization at 4.25-4.62 GHz, in addition to its small size, large bandwidth, and high gain. The suggested antenna is a promising option for sub-6GHz 5G applications.

III. CORPORATE FED ARRAY

Antenna gain required is not much increased since operating wavelengths in Sub 6 GHz are comparatively higher than those in higher frequency bands, such as the mm-wave and terahertz bands. The exact amount of antenna gain needed relies on a number of variables, including path loss, interference, and the required signal intensity. It also varies on the deployment scenario—urban, suburban, or rural—as well as the network's unique goals. Antenna gain plays a crucial role in influencing the coverage and connection performance as well as the effective isotropic radiated power (EIRP). However, in many sub-6 GHz installations, such as the 3.6 GHz band, an estimate of 0 to 6 dB is a fair value for the antenna gain. Antenna strengths between 0 and 6 dB are generally appropriate in urban and suburban settings, where small cells are frequently built for enhanced coverage and capacity. This makes it possible to balance link performance and coverage area well [27], [28]. As per [28], At 1 GHz, a −5dBi antenna gain is advised for user equipment. Increase the necessary gain in proportion to the frequency squared. This indicates that a gain of -2.2 dBi should be considered at 3.6 GHz and −1.6 dBi at 4.7 GHz for user equipment. Gain increases will result in a decrease in the input transmitting power needed for the gain. At 1GHz, a gain of 12 dBi and 7.5 dBi is advised for macrocells and microcells, respectively. As per [29], Antenna gains were often near unity (0 dBi / −2.1 dBi) at both 5 GHz and 6 GHz, but they might occasionally be as low as −6 dBi.

To increase gain, a four-element leaf-shaped antenna array is planned. Depending on the needed gain, the number of components may increase even more. When compared to a single antenna, a 4-element array can increase gain by up to three or four times in dB. Corporate feeding network is used to energize the radiating elements. Fig. 17(a), (b) and (c) show a simulated antenna's top and bottom views and fabricated prototype.

The 50 mm gap between four leaf-shaped elements enhances antenna size. To minimize array size, inter-element spacing is reduced, but mutual coupling is enhanced and antenna gain is diminished. Multiple hexagonal components

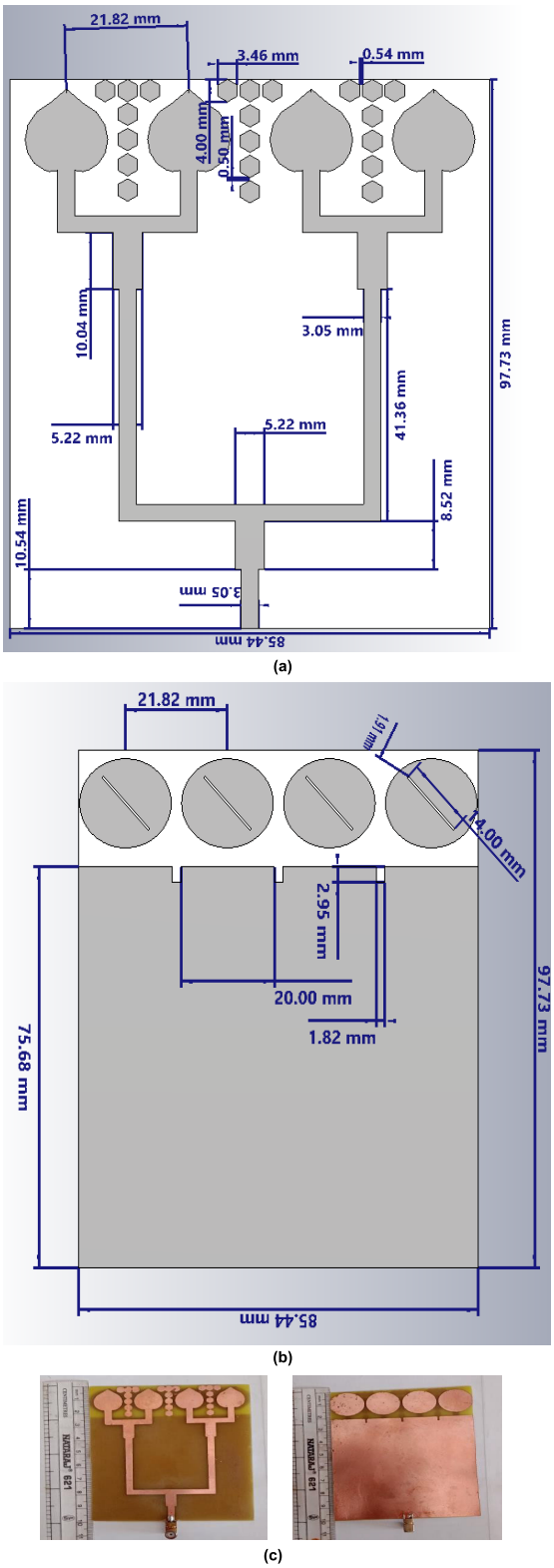

FIGURE 17. Proposed antenna's geometry (a) Top (b) Bottom (c) Fabricated prototype.

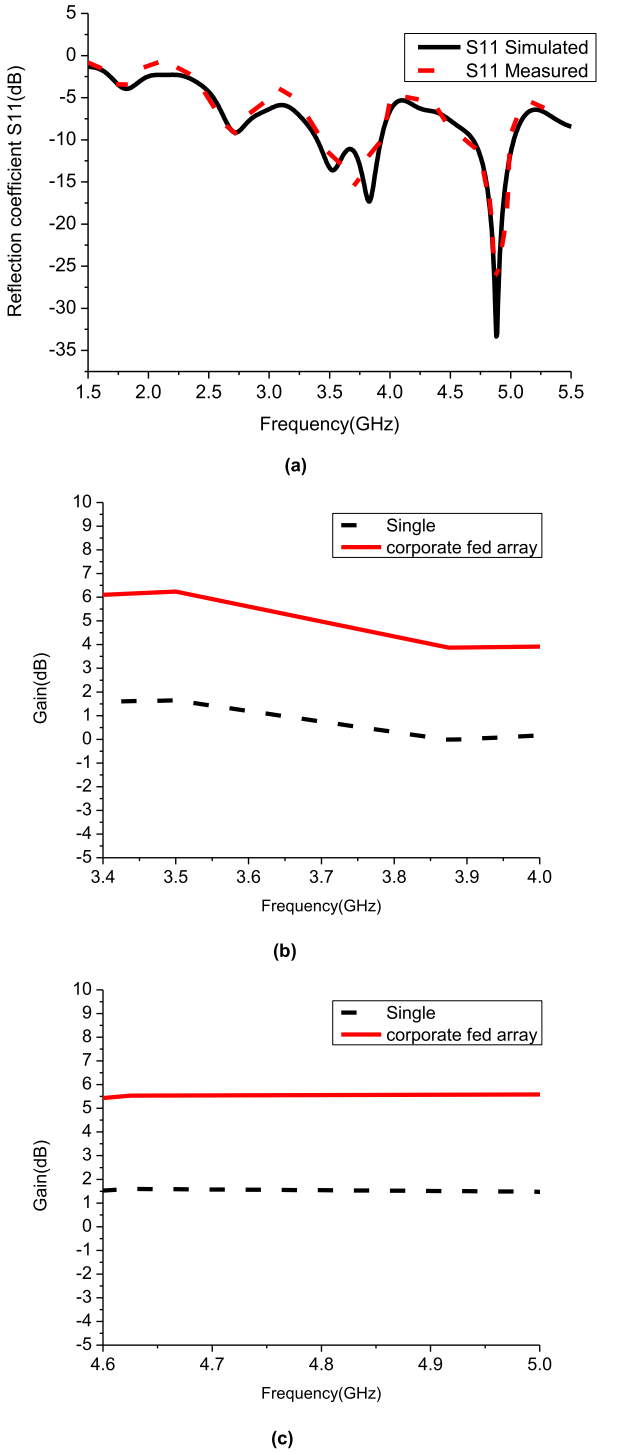

FIGURE 18. (a) Simulated and measured reflection coefficient (S11) variations with frequency of corporate fed array (b) Gain variations with frequency of corporate fed array in first operating band (c) Gain variations with frequency of corporate fed array in second operating band.

are inserted in T-shaped between inter-elements to decrease surface wave and reduce antenna size. This intermediate structure acts as a decoupling element and band-stop filter, boosting antenna gain by reducing mutual coupling. Corporate feed network supplies radiating elements. Matching microstrip lines and quarter-wave transformers provide a 1:4 power divider. 50 Ohm microstrip lines feed all patches. Impedance is reduced (25 Ohm) at the T point where two

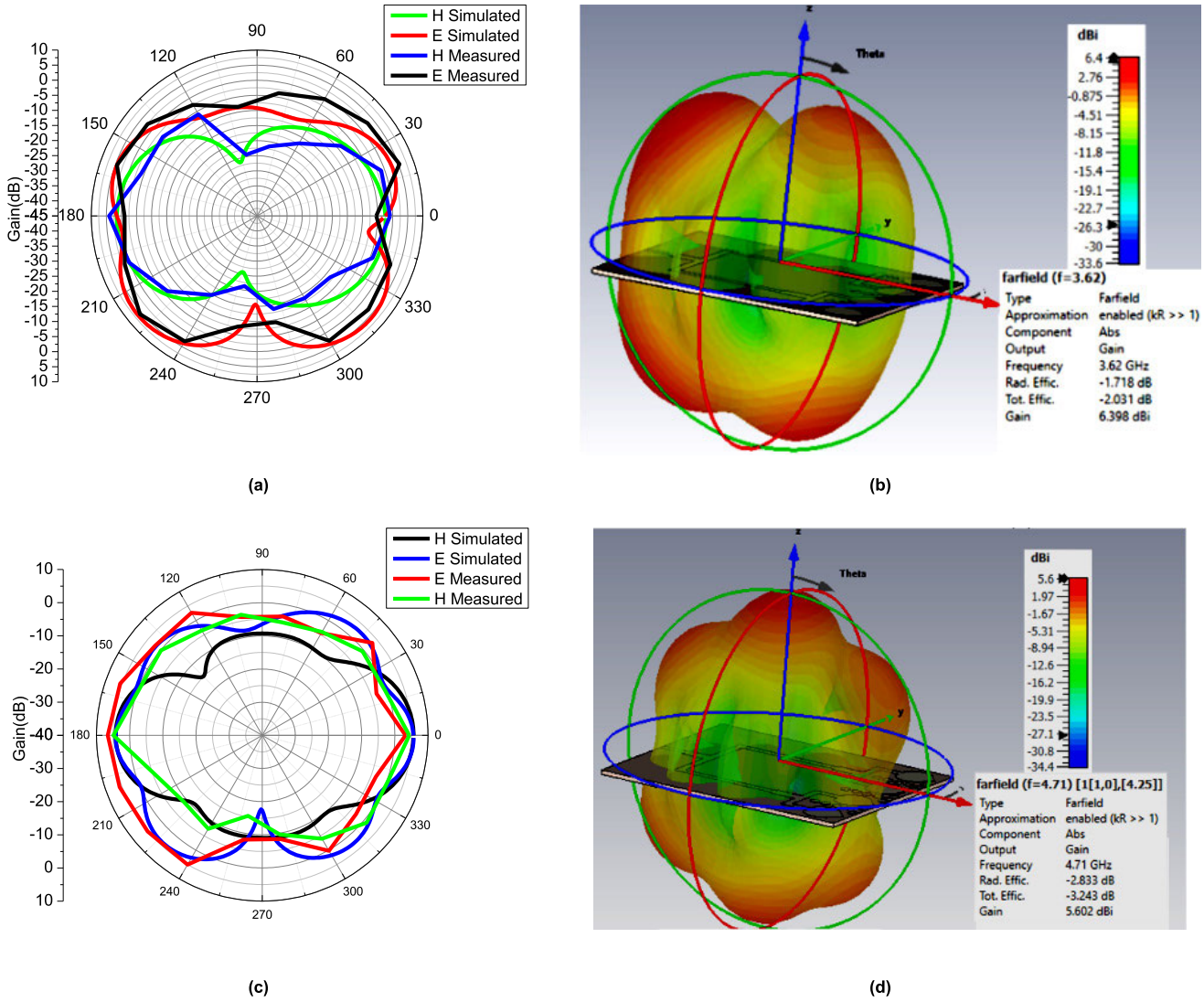

FIGURE 19. (a) 2D Radiation pattern at 3.6 GHz (b) 3D Radiation pattern at 3.6 GHz (c) 2D Radiation pattern at 4.71 GHz (d) 3D Radiation pattern at 4.71 GHz.

feed lines are joined. The T point is linked to a new 50 ohm microstrip line via a quarter wave transformer with 35.35 Ohm ($\sqrt{}$ (50 × 25)) impedances. Every T-point is the same. First, length of connected microstrip lines are half the guided wavelength or odd multiples. These lengths are then adjusted to optimize performance and size. The proposed antenna is simulated using CST Microwave Studio.

Fig. 18(a) shows the proposed antenna's simulated and measured Reflection coefficient (S11) variations with frequency. The simulated antenna operates between 3.4-4 GHz and 4.65-5.05 GHz with Reflection coefficient (S11) less than -10 dB, whereas the constructed antenna operates from 3.43 to 3.9 GHz and 4.61 to 4.99 GHz, covering the sub-6 GHz band for 5G connection. The measured Reflection coefficient (S11) and resonant frequency feature variations due to manufacturing imperfections on the patch and ground plane. Due to the numerous power dividers involved in the feeding network, the corporate fed array's bandwidth is reduced in both bands (as shown in Fig. 18(a)), but it covers the essential sub-6 GHz spectrum for 5G connectivity.

The gain of the suggested antenna is shown in Fig. 18(b) and (c) for first band and second band. The gain of a corporate-fed array is 3.95 dB at 3.6 GHz and 5 dB at 4.7 GHz. Gain fluctuates by less than 3 dB throughout all operational bands. A corporate fed array offers about 4 dB more gain than a single element.

Fig.19 (a) and (c) show measured and simulated E and H field radiation patterns at 3.6 and 4.71 GHz. Three dimensional radiation pattern at 3.6 and 4.71 GHz is depicted in Fig. 19 (b) and (d) respectively. The shapes of the simulated and measured patterns are comparable but some variations due to manufacturing imperfections and inadequate solder connections, but the orientations of the principal lobes are identical. Maximum gain at 3.6 GHz and 4.71 GHz is

6.39 dB and 5.64 dB for simulated antenna and 5.67 dB and 6.56 dB for observed antenna. Numerous large lobes with a maximum gain of 6.4 dB are seen in the pattern shown in Fig. 19(b) at 3.6 GHz. Major Lobes are associated with the top and bottom planes of the antenna, whereas side lobes are small. It should be noted from Fig. 19(d) that the antenna offers sufficient coverage by using three major lobes on its upper and lower planes at 4.7 GHz. The proposed antenna array generates the least amount of end fire-directed radiation.

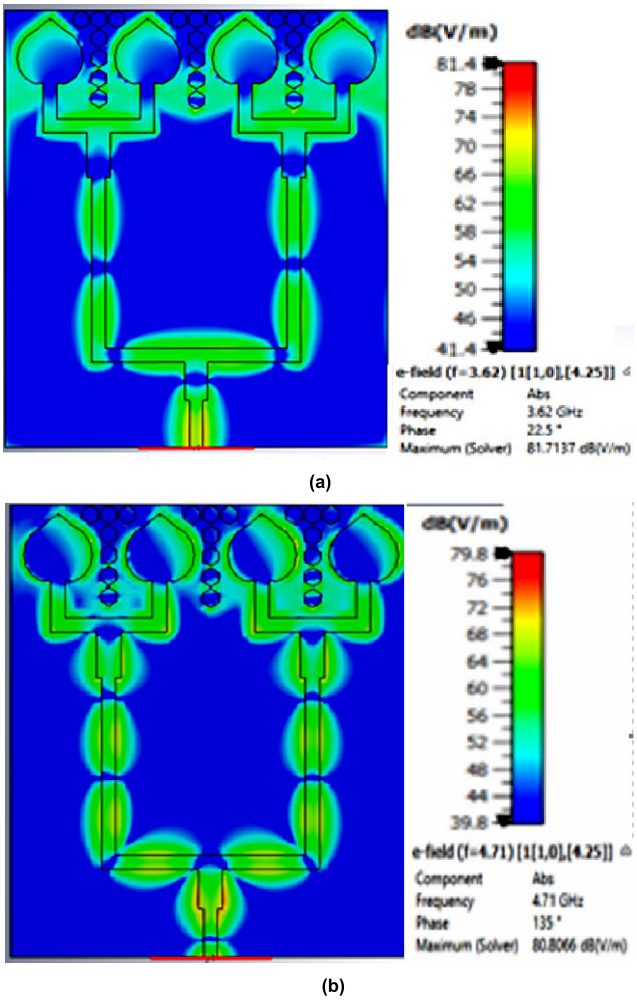

FIGURE 20. E-field distribution of corporate fed 4 × 1 array of leaf shaped antenna (a) at 3.6 GHz (b) at 4.7 GHz.

The E-field distribution of a corporate-fed array of leaf-shaped antennas at 3.6 GHz and 4.71 GHz is shown in Figures 20(a) and (b), respectively. At 3.6 GHz and 4.7 GHz, the maximum E-field densities are 81.7 dB (V/m) and 80.8 dB (V/m), respectively. The E-field is widely distributed throughout the patch and the metallic disc at the bottom. At intermediate elements, the e-field is negligible.

Table 2 compares the proposed corporate fed array to the reported sub-6 GHz 5G antennas. In compared to existing published antennas, the suggested array has a small dimension, similar bandwidth, and good gain. 3.4-3.93 GHz and 4.65-5.05 GHz with Reflection coefficient (S11) less than -10 dB, whereas the constructed antenna operates from 3.43 to 4 GHz and 4.61 to 4.99 GHz,

TABLE 2. Performance comparisons of proposed corporate fed 4 × 1 array of leaf shaped antenna with reported sub 6 GHz MIMO antennas.

Work	Size (mm^3)	Frequency range (GHz)	Impedance Bandwidth (%) (S11<10)	Max. gain (dB)
Proposed corporate fed 4×1 array of leaf shaped antenna (Observed)	85×97.73 ×1.6	3.43-3.9 4.61-4.99	13.05 8.08	6.56
Proposed corporate fed 4×1 array of leaf shaped antenna (Modeled)	85×97.73 ×1.6	3.4-4 4.65-5.05	16.66 8.33	3.95
[30]	180×60× 1.6	3.28-3.78	14.28	2.4-6.1
[31]	100×100 ×5.7	3.39-3.62	6.57	5-6.8
[32]	150×80× 0.8	4.7-4.9	4.21	4.25-6
[33]	129.75×5 0×0.8	2.2-2.3 2.8-3.3 3.4-3.5	4.44 16.66 2.98	1.8-2.8

IV. MIMO ANTENNAS

A. SPATIAL DIVERSITY MIMO (SD-MIMO) ANTENNA

Future wireless communication systems will require MIMO antennas to boost network capacity. On CST, a two-element SD-MIMO configuration with a leaf-shaped antenna is modeled. Multiple antennas are positioned far enough apart to allow for the establishment of separate wireless links in spatial diversity MIMO antenna, which increases channel capacity. Multiple-input multiple-output (MIMO) techniques use transmitter arrays and receivers to add redundant operation, which improves error rates and boosts the efficiency of wireless systems. To construct a two-element MIMO antenna, two antenna elements are originally positioned at half wavelength distance, however the antenna dimension is enlarged due to the half wavelength gap. In order to reduce the dimension, two antennas are separated by 29.09 mm (less than half wavelength separation). I-shaped metallic element is put between inter-elements on the top layer to balance the mutual coupling. Fig. 21(a), (b) and (c) Simulated SD-MIMO top view, bottom view and fabricated prototype.

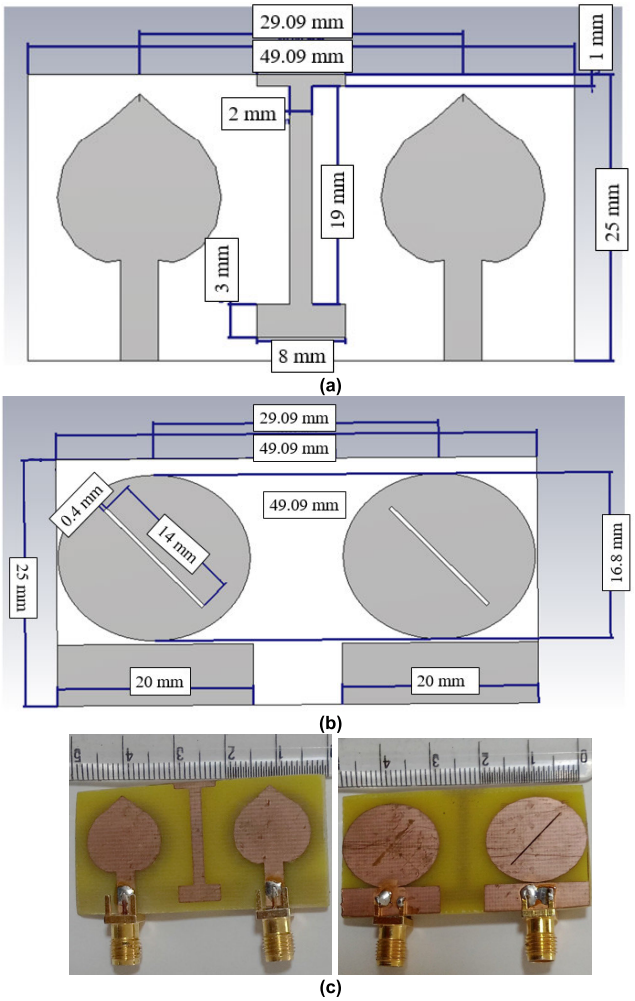

FIGURE 21. Structure of SD-MIMO configuration of leaf shaped antenna (a) Top view (b) Bottom view (c) Fabricated prototype.

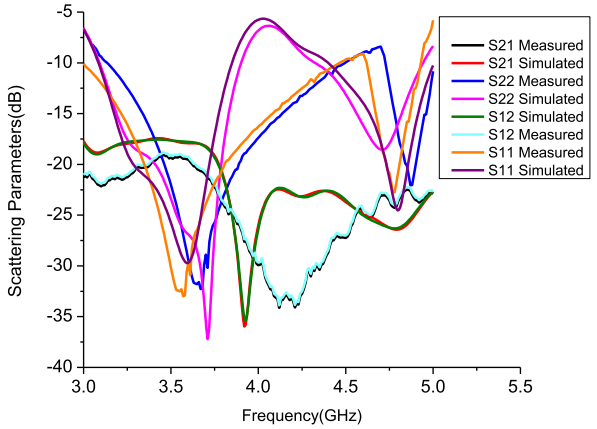

FIGURE 22. Observed and modeled S-parameters variations with frequency of spatial diversity antenna.

The S-Parameters variations with frequency of simulated and fabricated spatial diversity antenna is shown in Fig. 22. It shows that Reflection coefficient (S11) and S22 are nearly similar, while S12 and S21 are overlapping.

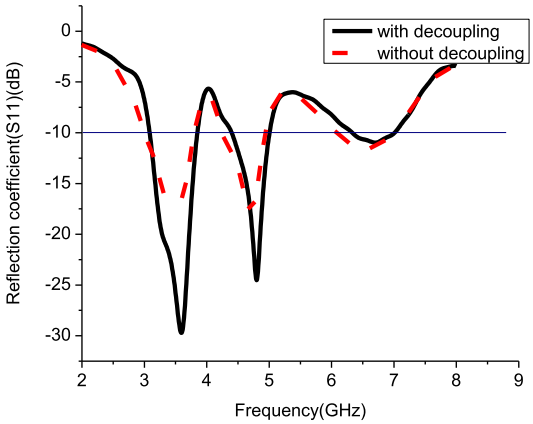

FIGURE 23. Comparative reflection coefficient (S11) variations with frequency of proposed SD-MIMO antenna with decoupling element and without decoupling element.

Simulated antenna is operating from 3.05-3.85 GHz and 4.4-5 GHz while fabricated antenna is operating from 3-4.4 GHz and 4.5-4.9 GHz. measured Reflection coefficient (S11) bandwidth. Simulated and measured minimum S21 is -36.5 dB and -34.5 dB respectively. There is a strong correlation between modeled and observed outcomes.

Fig. 23 represents the impact of decoupling elements on Reflection coefficient (S11) variations with frequency of antenna. It may be noted that bandwidth is almost unchanged while small shift in resonant frequencies are observed if decoupling elements are removed. Impedance matching performance or return loss is increased in absence of decoupling elements. In presence of decoupling elements, Reflection coefficient (S11) is about -30 dB and -24 dB at 3.6 GHz and 4.7 GHz. Decoupling elements improve impedance matching by reducing the interaction between inter-elements.

Fig. 24 depicts the influence of decoupling element on the antenna's isolation ability. Using decoupling element isolation is improved by about 10 dB and isolation bandwidth is increased. Decoupling elements block the radiation transmits between inter-elements.

Fig. 25 depicts the influence of inter-element separation on Reflection coefficient (S11). For the separation of 0.3λ, the maximum bandwidth is reached in the lower band, but the second resonance shifts. At 0.4λ and 0.5λ separation, the maximum bandwidth is reached for both bands. For dimension reduction, separation of 0.4λ is used.

Fig. 26 represents the effect of antenna's separation on the mutual coupling. Mutual coupling decreases as separation increases, and isolation bandwidth increases. To achieve maximum Reflection coefficient (S11) bandwidth and isolation bandwidth with compact dimension, spacing of 0.4λ is chosen.

When port 1 of the proposed spatial diversity antenna is linked to the RF reception circuit in an anechoic room and

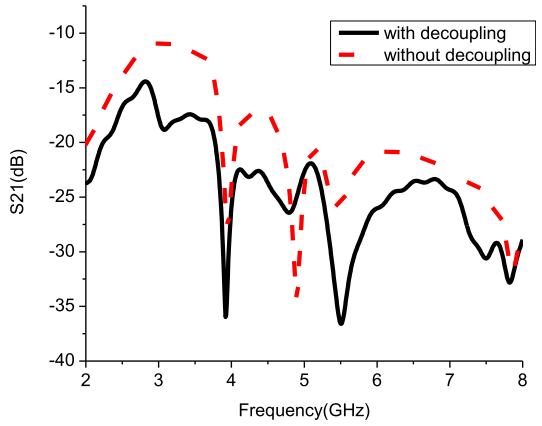

FIGURE 24. Comparative S21 variations with frequency of proposed SD-MIMO antenna (spacing 0.4 × 72.72) with decoupling element and without decoupling element.

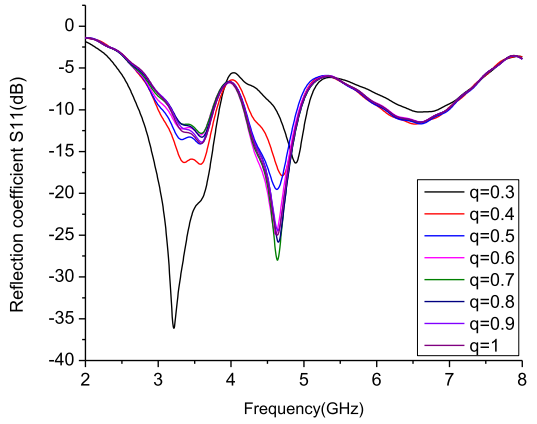

FIGURE 25. Comparative reflection coefficient (S11) variations with frequency of proposed SD-MIMO antenna with different element-separation's (q×72.72 mm).

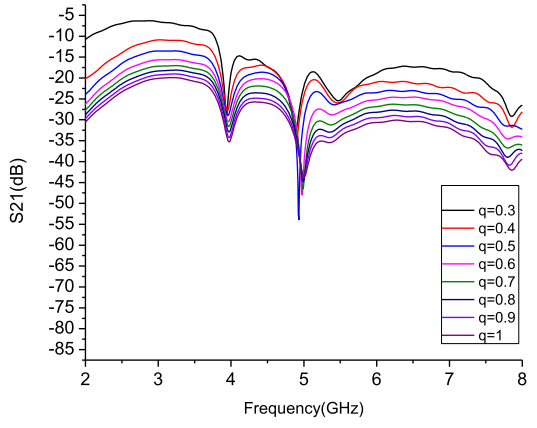

FIGURE 26. Comparative mutual coupling(S21) variations with frequency of proposed SD-MIMO antenna with different element-separation's (q×72.72 mm).

port 2 is attached with 50 ohm matched impedance, the radiation characteristics is monitored. Fig. 27 (a) and (b) shows the observed and modeled E field and H field patterns of the antenna at 3.6 GHz and 4.7 GHz. It may be noted

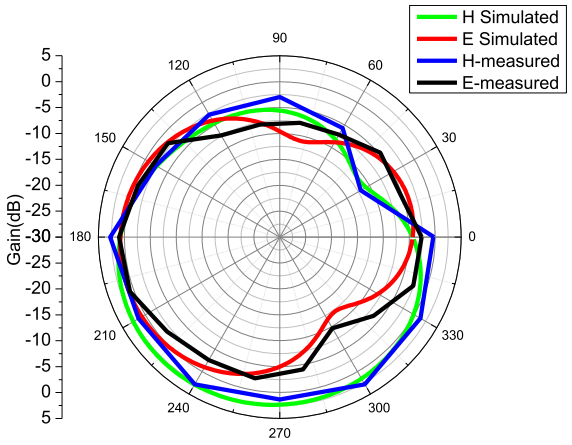

(a)

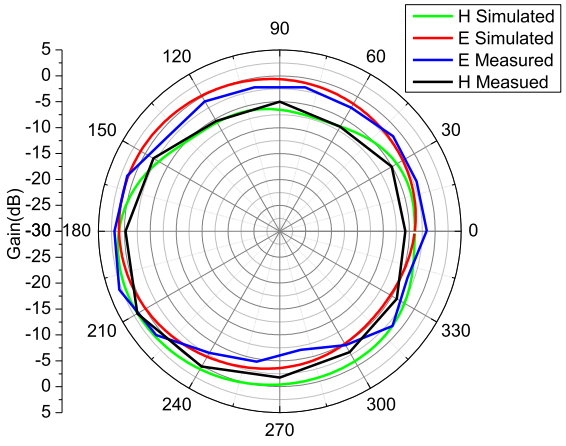

(b)

FIGURE 27. Observed and modeled radiation characteristics of spatial diversity antenna (a) at 3.6 GHz (b) at 4.76 GHz.

that the observed and modeled radiation characteristics are very similar. Simulated and Measured gain of antenna 2.9 dB and 2.8 dB at 3.6 GHz while it is 1.75 dB and 1.712 dB at 4.7 GHz. The direction of maximum is altered, but the form is essentially same. Variations between observed and modeled values are attributable to manufacture defects, port solder joints, etc.

Fig. 28 (a) and (b) depict the E-field distribution of the spatial diversity antenna at 3.62 GHz when port 1 and port 2, correspondingly, are stimulated. Fig. 28 (c) and (d) depict the E-field distribution at 4.7 GHz when port 1 and port 2, correspondingly, are activated. When port 1 is stimulated, there is a weak E-field at the neighboring element due to the decoupling element. When port 2 is activated, something similar occurs. At 3.62 GHz, the maximum E-field densities are 90.2 dB (V/m) for port 1 stimulation and 89.48 dB (V/m) for port 2 stimulation. At 3.62 GHz, the maximum E-field densities are 90.184 dB (V/m) for port 1 stimulation and 89.5 dB (V/m) for port 2 stimulation. Maximum E-field densities at 4.7 GHz are 88.1 dB (V/m) for

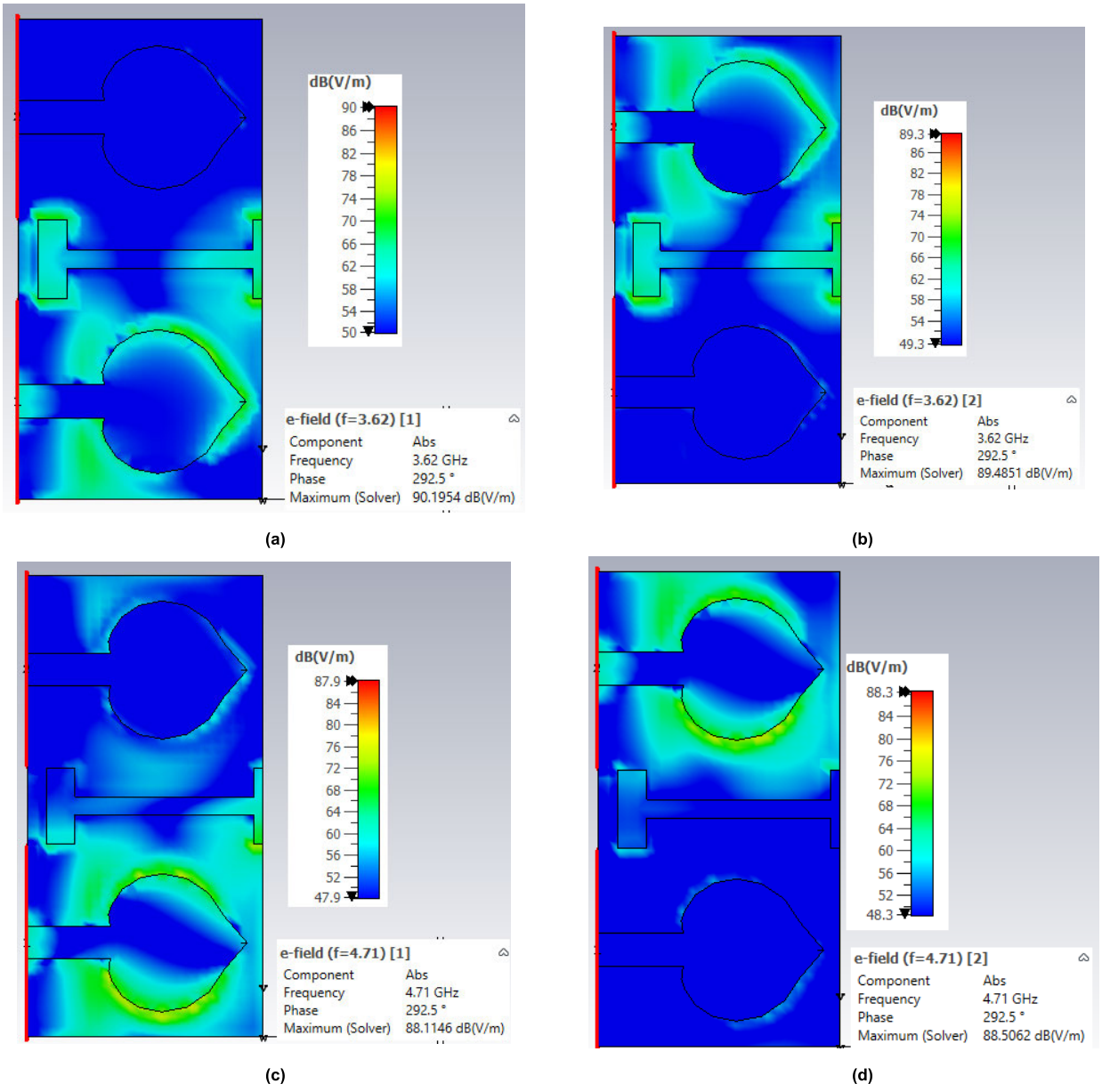

FIGURE 28. E-field distribution of proposed spatial diversity antenna (a) when port 1 is excited at 3.62 GHz (b) when port 2 is excited at 3.62 GHz (c) when port 1 is excited at 4.7 GHz (d) when port 2 is excited at 4.7 GHz.

port 1 stimulation and 88.5 dB (V/m) for port 2 stimulation, respectively.

Fig. 29 shows various MIMO performance parameters of proposed spatial diversity antenna. Fig. 29 represents MEG (Mean effective gain), DG (Diversity gain), ECC (Envelope Correlation Coefficient), CCL (Channel capacity loss) and TARC (Total active reflection coefficient) variations with frequency respectively. It can be seen that DG is extremely near to 10 in both operational bands. ECC is near to zero in both operating bands, indicating that both antennas work independently. MEG1 and MEG2 are practically identical, So MEG is close to zero in the initial band and less than 0.4 dB in the second, showing that the proposed antenna supports efficient MIMO operations. CCL is smaller than 0.5 bit/sec/Hz over the frequency range of operation, demonstrating low communication losses. TARC is less than 0 dB throughout the entire operating spectrum. The TARC minimum at 3.6 GHz is −9.5 dB and at 4.7 GHz, it is −11 dB.

B. PATTERN DIVERSITY MIMO (PD-MIMO) ANTENNA

Pattern diversity in two elements MIMO antenna of leaf shape is built by orthogonally putting two components with horizontal spacing of 35.20 mm and vertical separation of 35.20 mm. Fig. 30 (a), (b) and (c) depict the antenna's top and bottom perspectives, respectively.

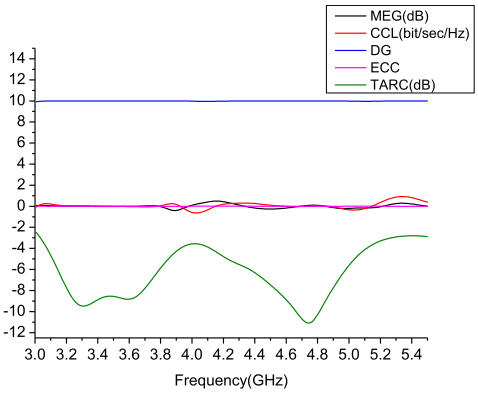

FIGURE 29. MIMO parameters of proposed spatial diversity antenna: (Mean effective gain (MEG), Channel capacity loss (CCL), Diversity gain (DG), Envelope correlation coefficient (ECC), and Total active reflection coefficient (TARC).

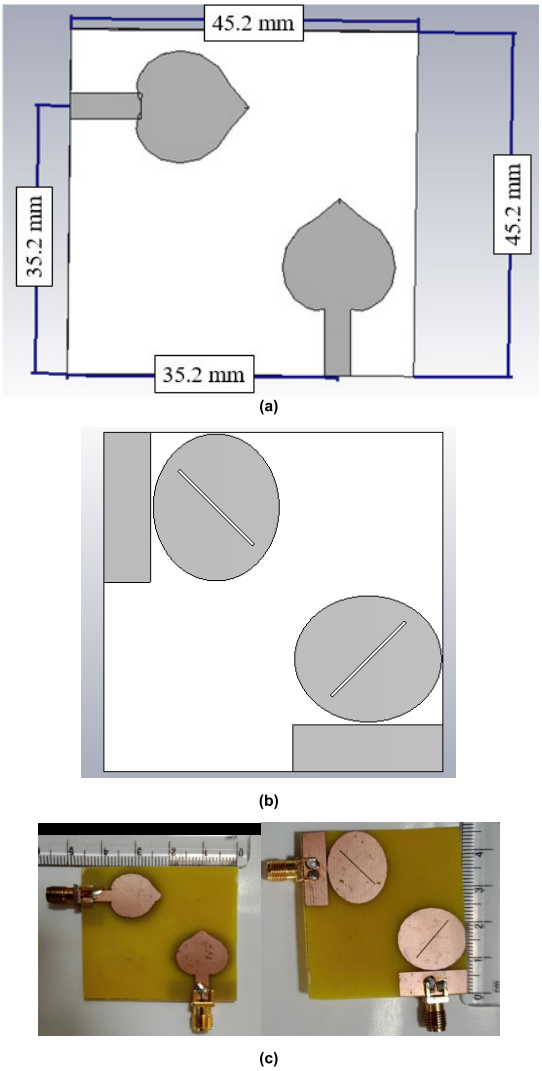

FIGURE 30. Proposed pattern diversity antenna (a) Top view (b) Bottom view (c) Fabricated prototype.

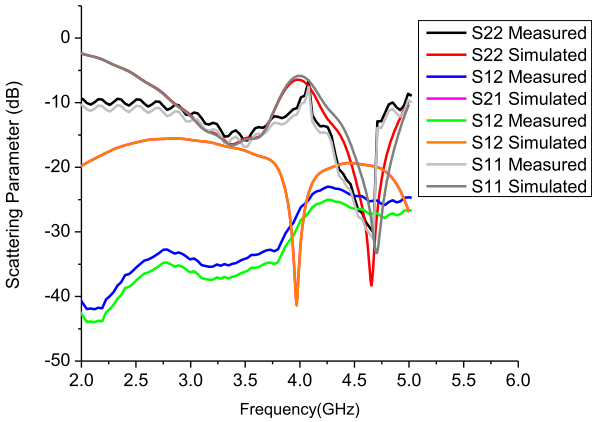

FIGURE 31. Observed and modelled scattering parameter variations with frequency of pattern diversity antenna.

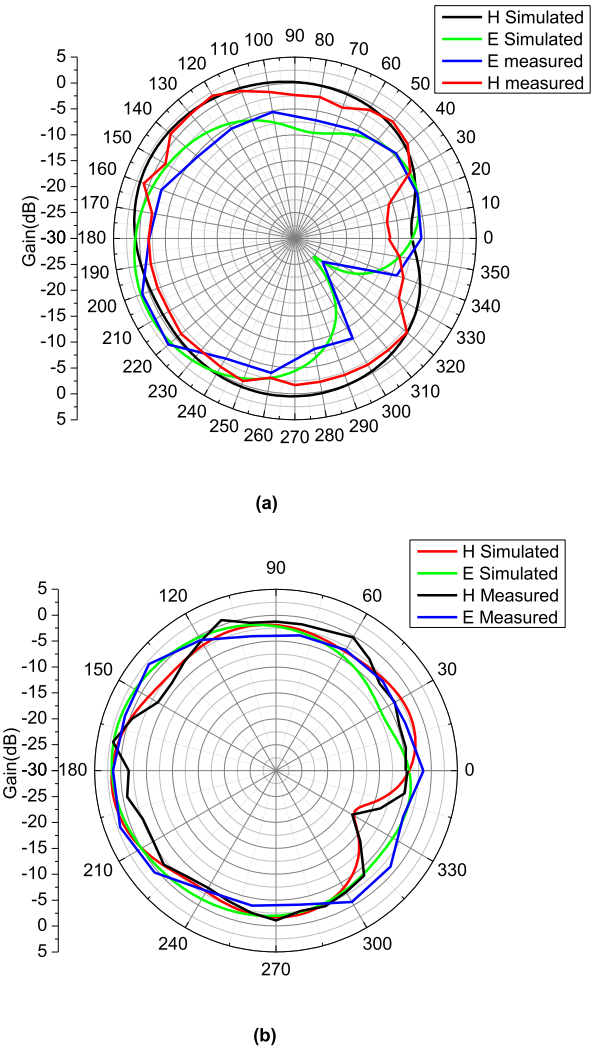

FIGURE 32. Observed and modeled radiation characteristics of pattern diversity antenna (a) at 3.6 GHz (b) at 4.76 GHz.

The scattering parameter observed and modelled is shown variations with frequency in Fig. 31. Simulated antenna operates between 2.8-3.8 GHz and 4.3-5 GHz while fabricated antenna operates between 2.8-4 GHz and 4.1-5GHz.

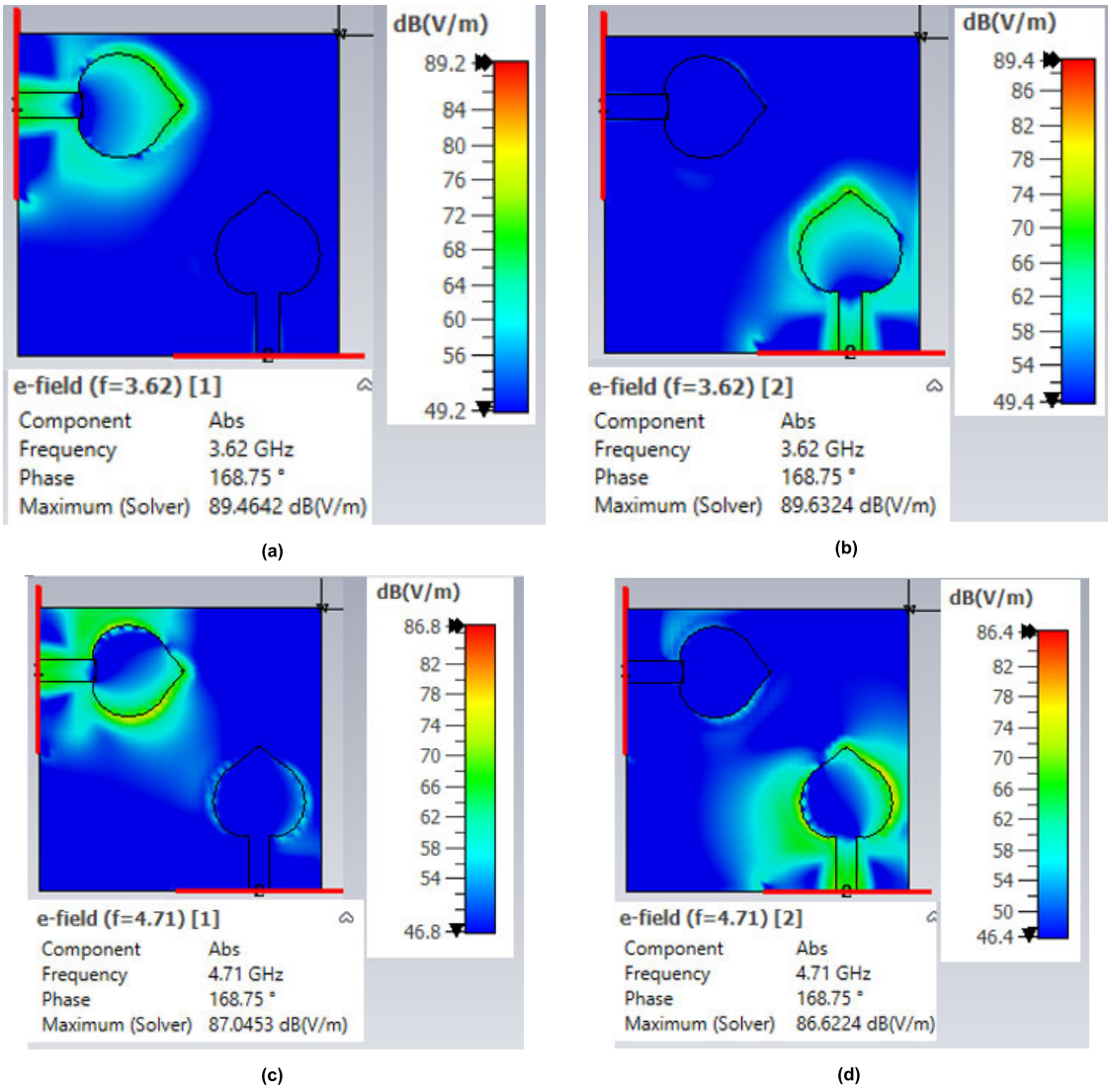

FIGURE 33. E-field distribution of proposed pattern diversity antenna (a) when port 1 is energized at 3.6 GHz (b) when port 2 is energized at 3.6 GHz (c) when port 1 is energized at 4.7 GHz (b) when port 2 is energized at 4.7 GHz.

Fig. 32 (a) and (b) depicts the modeled and observed radiation characteristics of the pattern diversity antenna at 3.6 GHz and 4.76 GHz. Simulated and measered maximum gain are 1.6 dB and 1.8 dB respectively at 3.6 GHz while they are 1.8 dB and 2 dB at 4.76 GHz.

Fig. 33 (a) and (b) depict the E-field distribution of the proposed antenna when port 1 and port 2 are respectively, energized at 3.62 GHz. Fig. 33 (c) and (d) illustrate the E-field distribution of the proposed antenna at 4.7 GHz when port 1 and port 2 are enabled, respectively. When port 1 is stimulated, it is evident that the E-field at the neighboring element is negligible. When port 2 is activated, something similar occurs. At 3.62 GHz, the maximum E-field densities are 89.4 dB (V/m) for port 1 stimulation and 89.6 dB (V/m) for port 2 stimulation. Maximum E-field densities at 4.7 GHz are 87.0 dB (V/m) for port 1 stimulation and 86.6 dB (V/m) for port 2 stimulation, respectively.

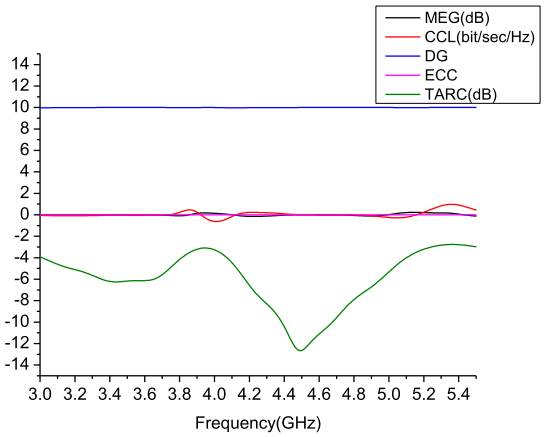

FIGURE 34. MIMO parameters of proposed pattern diversity antenna.

Fig. 34 shows various MIMO performance parameters of proposed pattern diversity antenna. Fig. 34 represents

DG, ECC, MEG, CCL and TARC variations with frequency respectively. All the parameters in acceptable range.

C. PERFORMANCE COMPARISION WITH REPORTED ANTENNAS

In the Table 3, recommended MIMO antenna performance is compared to reported MIMO antenna performance. Compared to previously published antennas, the proposed SD-MIMO and PD-MIMO antenna have a large bandwidth, a compact dimension, and excellent MIMO features. The suggested antennas are relatively compact.

TABLE 3. Performance comparisons of proposed MIMO antennas with reported sub 6 GHz MIMO antennas.

Performance Parameters	Proposed SD-MIMO (Modeled)	Proposed PD-MIMO (Modeled)	[34]	[35]	[36]	[37]
Size mm^3	49.09× 25× 1.6	45.20× 45.20× 1.6	160× 70× 0.787	60× 60× 0.8	70× 126× 4.27	30× 6.75× 0.32
Work Freq. range (GHz)	3.05-3.85 4.4-5	2.3-3.8 4.3-5	5.55-5.6	3.15 3.56-4	5.8	4.9-5.06
Bandwidth (GHz)	0.8 0.6	1.5 0.7	0.05	0.1 0.04	0.5	0.16
S21 (dB)	-17 -25	-17 -20	<-40	<-20	<-31	-22
DG	10	10	10	-	9.99	9.6
ECC	0	<0.005	<0.005	<0.1	0.001	<0.05
CCL	<0.5	<0.1	-	-	-	-
TARC	-9 -11	-7 -12.5	-	-	-	-
MEG (dB)	<0.2	<0.1	-	-3 to 3	-	-

V. CONCLUSION

Various antennas operating in the sub-6 GHz range have been proposed for use in the following 5G bands: N77 (3.3–4.2 GHz), N78 (3.3–3.8 GHz), and N79 (4.7 GHz) (4.4–5 GHz). A single leaf-shaped antenna has a compact size of 25∗20∗1.6 mm3 ($0.24\lambda \times 0.20\ \lambda \times 0.015\ \lambda$) and a maximum gain of 1.6 dB with less than 3 dB variation across the operating band. A 4 × 1 array of optimized leaf-shaped radiating elements is described, with 13.15 percent bandwidth at 3.6 GHz and 3.95 dB gain and 8.33 percent bandwidth at 4.7 GHz and 5 dB gain. Gain variations are fewer than 3 dB across the working bandwidth. Pattern diversity and SD-MIMO designs with good bandwidth, high gain, minimal mutual coupling, and acceptable MIMO parameters have been proposed. The proposed antennas are compatible with 5G devices and 5G base stations. In addition, it may be used for a variety of applications, including healthcare, health monitoring, IoT, the military, wireless body area networks, industrial automation, etc.

ACKNOWLEDGMENT

The authors would like to thank the ECE Department, Manipal University, Jaipur, for providing laboratory facilities and CST software, also would like to thank the Swami Keshwanand Institute of Technology, Jaipur, for their support in fabrication. Their appreciation extends to the ECE Department, Government Mahila Engineering College, Ajmer, for providing measurement facilities. Their contributions were pivotal to the success of our research, and also would like to thank the collaborative support from these institutions.

REFERENCES

[1] J. Acharjee, R. L. Kumar, K. Mandal, and S. K. Mandal, "A compact multiband multimode antenna employing defected ground structure," *Radioengineering*, vol. 28, no. 4, pp. 663–670, Dec. 2019.

[2] T. Nahar and S. Rawat, "Efficiency enhancement techniques of microwave and millimeter-wave antennas for 5G communication: A survey," *Trans. Emerg. Telecommun. Technol.*, vol. 33, no. 9, p. e4530, Sep. 2022, doi: 10.1002/ett.4530.

[3] H. Wong, K.-M. Luk, C. H. Chan, Q. Xue, K. K. So, and H. W. Lai, "Small antennas in wireless communications," *Proc. IEEE*, vol. 100, no. 7, pp. 2109–2121, Jul. 2012, doi: 10.1109/JPROC.2012.2188089.

[4] G. Adamiuk, T. Zwick, and W. Wiesbeck, "UWB antennas for communication systems," *Proc. IEEE*, vol. 100, no. 7, pp. 2308–2321, Jul. 2012, doi: 10.1109/JPROC.2012.2188369.

[5] S. Vitturi, C. Zunino, and T. Sauter, "Industrial communication systems and their future challenges: Next-generation Ethernet, IIoT, and 5G," *Proc. IEEE*, vol. 107, no. 6, pp. 944–961, Jun. 2019, doi: 10.1109/JPROC.2019.2913443.

[6] J. Restrepo. (2019). *Spectrum Allocation for 5G International Framework*. [Online]. Available: https://www.itu.int/en/ITU-D/Regulatory-Market/Pages/Events2019/Togo/5Gworkshop.aspx

[7] R. Azim, R. Aktar, A. K. M. M. H. Siddique, L. C. Paul, and M. T. Islam, "Circular patch planar ultra-wideband antenna for 5G sub-6 GHz wireless communication applications," *J. Optoelectron. Adv. Mater.*, vol. 23, nos. 3–4, pp. 127–133, 2021.

[8] M. Agiwal, A. Roy, and N. Saxena, "Next generation 5G wireless networks: A comprehensive survey," *IEEE Commun. Surveys Tuts.*, vol. 18, no. 3, pp. 1617–1655, 3rd Quart., 2016, doi: 10.1109/COMST.2016.2532458.

[9] *A White Paper on Enabling 5G in India*, Telecom Regulatory Authority India (TRAI), New Delhi, India, 2019.

[10] G. Jin, C. Deng, Y. Xu, J. Yang, and S. Liao, "Differential frequency-reconfigurable antenna based on dipoles for sub-6 GHz 5G and WLAN applications," *IEEE Antennas Wireless Propag. Lett.*, vol. 19, pp. 472–476, 2020, doi: 10.1109/LAWP.2020.2966861.

[11] P. Liu, Z. Meng, L. Wang, Y. Zhang, and Y. Li, "Omnidirectional dual-polarized saber antenna with low wind drag," *IEEE Trans. Antennas Propag.*, vol. 68, no. 1, pp. 558–563, Jan. 2020, doi: 10.1109/TAP.2019.2934566.

[12] C.-Y. Hsieh, C.-H. Wu, and T.-G. Ma, "A compact dual-band filtering patch antenna using step impedance resonators," *IEEE Antennas Wireless Propag. Lett.*, vol. 14, pp. 1056–1059, 2015, doi: 10.1109/LAWP.2015.2390033.

[13] Q. L. Li, S. W. Cheung, D. Wu, and T. I. Yuk, "Optically transparent dual-band MIMO antenna using micro-metal mesh conductive film for WLAN system," *IEEE Antennas Wireless Propag. Lett.*, vol. 16, pp. 920–923, 2017, doi: 10.1109/LAWP.2016.2614577.

[14] A. R. Jalali, J. Ahamdi-Shokouh, and S. R. Emadian, "Compact multiband monopole antenna for UMTS, WiMAX, and WLAN applications," *Microw. Opt. Technol. Lett.*, vol. 58, no. 4, pp. 844–847, Apr. 2016, doi: 10.1002/mop.29685.

[15] Y. Bar-Cohen, *Biomimetics: Biologically Inspired Technologies*. Boca Raton, FL, USA: CRC Press, 2005, doi: 10.1201/9780849331633.

[16] A. J. R. Serres, G. K. de Freitas Serres, P. F. da Silva Júnior, R. C. S. Freire, J. do Nascimento Cruz, T. C. de Albuquerque, M. A. Oliveira, and P. H. da Fonseca Silva, "Bio-inspired microstrip antenna," in *Microstrip Antennas*, S. Chattopadhyay, Ed., Rijeka, Croatia: IntechOpen, 2017, doi: 10.5772/intechopen.69766.

[17] U. Keshwala, S. Rawat, and K. Ray, "Plant shaped antenna with trigonometric half sine tapered leaves for THz applications," *Optik*, vol. 223, Dec. 2020, Art. no. 165648, doi: 10.1016/j.ijleo.2020.165648.

[18] P. Singh, K. Ray, and S. Rawat, "Nature inspired sunflower shaped microstrip antenna for wideband performance," *Int. J. Comput. Inf. Syst. Ind. Manag. Appl.*, vol. 9, no. 2017, pp. 1–8, 2017. [Online]. Available: http://www.mirlabs.org/ijcisim/regular_papers_2016/IJCISIM_36.pdf

[19] U. Keshwala, S. Rawat, and K. Ray, "Bio-inspired lotus (*Nelumbo nucifera*) shaped ultra-wide band planar antenna for wireless applications," in *Proc. Int. Conf. Opt. Wireless Technol.*, 2022, pp. 417–424, doi: 10.1007/978-981-19-1645-8_43.

[20] U. Keshwala, S. Rawat, and K. Ray, "Nature inspired dual band sneezewort plant growth pattern shaped antenna," in *Proc. IEEE Asia–Pacific Microw. Conf. (APMC)*, Nov. 2017, pp. 580–583, doi: 10.1109/APMC.2017.8251512.

[21] T. Nahar and S. Rawat, "Survey of various bandwidth enhancement techniques used for 5G antennas," *Int. J. Microw. Wireless Technol.*, vol. 14, no. 2, pp. 204–224, Mar. 2022, doi: 10.1017/s1759078720001804.

[22] E. F. O'Connor and J. J. Robertson. *Cardioid*. MacTutor Hist. Math. Archive, Univ. St Andrews. Accessed: Jun. 14, 2022. [Online]. Available: https://mathshistory.st-andrews.ac.uk/Curves/Cardioid/

[23] N. Kulkarni, R. M. Linus, and N. B. Bahadure, "A small wideband inverted l-shaped flexible antenna for sub-6 GHz 5G applications," *AEU-Int. J. Electron. Commun.*, vol. 159, Feb. 2023, Art. no. 154479, doi: 10.1016/j.aeue.2022.154479.

[24] H. Shi, X. Zhang, J. Li, P. Jia, J. Chen, and A. Zhang, "3.6-GHz eight-antenna MIMO array for mobile terminal applications," *AEU-Int. J. Electron. Commun.*, vol. 95, pp. 342–348, Oct. 2018, doi: 10.1016/j.aeue.2018.09.008.

[25] A. Boukarkar, S. Rachdi, M. M. Amine, B. Sami, and A. B. Khalil, "A compact four states radiation-pattern reconfigurable monopole antenna for sub-6 GHz IoT applications," *AEU-Int. J. Electron. Commun.*, vol. 158, Jan. 2023, Art. no. 154467, doi: 10.1016/j.aeue.2022.154467.

[26] A. T. Z. Moses and N. Moses, "Compact self decoupled MIMO antenna pairs covering 3.4–3.6 GHz band for 5G handheld device applications," *AEU-Int. J. Electron. Commun.*, vol. 141, Nov. 2021, Art. no. 153971, doi: 10.1016/j.aeue.2021.153971.

[27] *Unlicensed Use of the 6 GHz Band, Report and Order and Further Notice of Proposed Rulemaking*, Federal Commun. Commission, Washington, DC, USA, 2020.

[28] *5G Spectrum Scenarios, Requirements and Technical Aspects for Bands Above 6 GHz*, METIS-II/5GPPP, U.K., 2016, pp. 1–57.

[29] *6 GHz Unlicensed Spectrum Regulations and Deployment Options*, CISCO Syst. Pte. Ltd., Singapore, 2023.

[30] Z. An and M. He, "A simple planar antenna for sub-6 GHz applications in 5G mobile terminals," *Appl. Comput. Electromagn. Soc. J.*, vol. 35, no. 1, pp. 10–15, 2020.

[31] G. Jin, C. Deng, J. Yang, Y. Xu, and S. Liao, "A new differentially-fed frequency reconfigurable antenna for WLAN and sub-6GHz 5G applications," *IEEE Access*, vol. 7, pp. 56539–56546, 2019, doi: 10.1109/ACCESS.2019.2901760.

[32] M. Khalifa, L. Khashan, H. Badawy, and F. Ibrahim, "Broadband printed-dipole antenna for 4G/5G smartphones," *J. Phys., Conf. Ser.*, vol. 1447, no. 1, Jan. 2020, Art. no. 012049, doi: 10.1088/1742-6596/1447/1/012049.

[33] N. Sekeljic, Z. Yao, and H.-H. Hsu, "5G broadband antenna for sub-6 GHz wireless applications," in *Proc. IEEE Int. Symp. Antennas Propag. USNC-URSI Radio Sci. Meeting*, Jul. 2019, pp. 147–148, doi: 10.1109/APUSNCURSINRSM.2019.8888509.

[34] J. Khan, S. Ullah, F. A. Tahir, F. Tubbal, and R. Raad, "A sub-6 GHz MIMO antenna array for 5G wireless terminals," *Electronics*, vol. 10, no. 24, p. 3062, Dec. 2021, doi: 10.3390/electronics10243062.

[35] D. Sarkar and K. V. Srivastava, "Four element dual-band sub-6 GHz 5G MIMO antenna using SRR-loaded slot-loops," in *Proc. 5th IEEE Uttar Pradesh Sect. Int. Conf. Electr., Electron. Comput. Eng. (UPCON)*, Nov. 2018, pp. 1–5, doi: 10.1109/UPCON.2018.8596789.

[36] A. S. M. Alqadami, M. F. Jamlos, P. J. Soh, and G. A. E. Vandenbosch, "Assessment of PDMS technology in a MIMO antenna array," *IEEE Antennas Wireless Propag. Lett.*, vol. 15, pp. 1939–1942, 2016, doi: 10.1109/LAWP.2015.2513960.

[37] I. S. Masoodi, I. Ishteyaq, and K. Muzaffar, "Extra compact two element sub 6 Ghz MIMO antenna for future 5G wireless applications," *Prog. Electromagn. Res. Lett.*, vol. 102, pp. 37–45, 2022, doi: 10.2528/pierl21100303.

TAPAN NAHAR received the Bachelor of Engineering (B.E.) degree in electronics and communication from the Global Institute of Technology, Jaipur, India, in 2009, the M.Tech. degree in digital communication from the Poornima College of Engineering, Jaipur, in 2015, and the Ph.D. degree in compact planar antennas for 5G from Manipal University, Jaipur. He is currently an Assistant Professor with the Department of Information and Communication Technology, Marwadi University, Rajkot, India. He is having experience of many years in teaching to undergraduate disciplines. He has to his credit several technical papers in international and national journals and conferences and books on various subjects.

SANYOG RAWAT received the Bachelor of Engineering (B.E.) degree in electronics and communication, the Master of Technology (M.Tech.) degree in microwave engineering, and Ph.D. degree in planar antennas. He is currently an Associate Professor and the Head of the Department of Electronics and Communication Engineering (ECE), Central University of Rajasthan, Kishangarh, Ajmer. He has been into teaching and research for more than 20 years. He has published more than 100 research papers in reputed journals and conferences and several book chapters. He has supervised eight Ph.D.'s till date and currently three are underway. He has supervised more than 30 M.Tech. dissertations work. His current research interests include RF and microwave devices, microstrip, and smart antennas and reconfigurable antennas. He has been a member of the technical program committee of many IEEE/Springer conferences and a reviewer of reputed journals like IEEE/Elsevier/Wiley/Springer. He has also edited the books on proceedings of the International Conference on Soft Computing Theories and Applications (SoCTA-2016 and 2017), Proceedings of International Conference on Smart Systems, Innovations and Computing (SSIC-2017) and International Conference on Engineering Vibrations, Communication, Information Processing (ICoEVCI, 2018), and International Conference for Wireless Communications (ICCWC-2021, 2022, and 2023) for Springer publication. He has extensively traveled to countries like Japan, Singapore, Malaysia, Vietnam, Indonesia, Thailand, and United Arab Emirates, to deliver talks, present research articles or in connection with other research/academic activities. He is a Life Fellow of the Institution of Electronics and Telecommunication Engineers (IETE), India; and a Life Member of Institution of Engineers (India), Indian Society for Technical Education (ISTE), and Indian Society of Lighting Engineers (ISLE) and Broadcast Engineering Society.

PARUL PATHAK received the B.E. degree in electronics and communication engineering, the M.Tech. degree in ECE, and the Ph.D. degree from RGPV Bhopal, India.

She is currently with the Department of Electronics and Communication Engineering, JECRC University, Jaipur. She has over 21 years of experience in teaching and research. She has presented several papers in national seminar/conferences and also published papers in national/international journals. Her research interests include microwave imaging, 5G communication, and RF energy harvesting. She is a technical reviewer for various international indexed journals of repute. She has been an invited speaker of many conferences, workshops, and faculty development programs. She is a member of various academic committees of different academic institutions.

PRAMOD KUMAR (Senior Member, IEEE) received the Bachelor of Engineering (B.E.) degree in electronics and communication, the Master of Technology (M.Tech.) degree in microwave engineering, and the Ph.D. degree in wireless sensor networks from NITK, Surathkal. He is currently a Professor with the Department of Electronics and Communication Engineering, Manipal Institute of Technology [a constituent unit of Manipal Academy of Higher Education (MAHE), Institute of Eminence]. He has been into teaching and research for more than 18 years. He has published over 60 research papers in reputed journals, conferences, and several book chapters. He has supervised two Ph.D.'s, and three are currently underway. He has supervised more than 20 M.Tech. dissertations work. He has been a member of the technical program committee of many IEEE/Springer conferences and a reviewer of reputed journals like IEEE/Elsevier/Wiley/Springer. He has also edited the books on proceedings of the International Conference for Wireless Communications (ICCWC-2021, 2022, and 2023) for Springer publication and IEEE and International Conference on Artificial Intelligence, Computational Electronics and Communication Systems (AICECS-2021 and 2023) of IOP: *Journal of Physics*. His current research interests include RF and microwave devices, microstrip and smart antennas, reconfigurable antennas, the IoT-based wireless sensor networks, and heart rate variability of ECG. He is a lifetime member of ISTE. He is the Organizing Chair of the IEEE conferences (e.g., AICECS 2024 and INCIP 2025). He has travelled extensively to countries like United Arab Emirates, Vietnam, Egypt, Jordan, Czech Republic, and Kathmandu to deliver talks, present research articles, or connect with other research/academic activities.

JAUME ANGUERA was born in Vinaròs, Spain, in 1972. He received the Ph.D. degree in telecommunications. He is currently a highly accomplished professional in the field of telecommunications. Holding various degrees in electronic systems, electronic engineering, and telecommunication engineering, he has a strong academic background. He is also the Founder and the CTO of Ignion and an Associate Professor with Universitat Ramon Llull, Barcelona, Spain. He has significantly contributed to the field. Throughout his career, he has been involved in ground breaking research on microstrip fractal-shaped antennas and has held key positions in renowned institutions and companies. Notably, he played a crucial role in developing cutting-edge antenna technologies with Fractus, where he was the Research and Development Manager and led projects for base station antennas, automotive, and mobile phones. With a prolific record, he has over 180 granted invention patents and has authored numerous journal articles, conference papers, and books. His pioneering work includes the invention of Antenna Booster Technology, commercially known as Virtual Antenna Technology. This technology has gained global adoption, facilitating wireless connectivity for IoT devices. Recognized for his achievements, he has received prestigious awards and honors, including European Information Technology Grand Prize and the New Faces of Engineering, in 2004. He is an IEEE Antennas and Propagation Distinguished Lecturer and serves as the Vice-Chair for the Working Group "Software and Modelling," EurAAP.